Title: Rubisco activity, electron transport rate, and leaf features drive high photosynthesis rate in the selected wild rice

Running Head: Efficient photosynthesis in the selected wild rice

Jyotirmaya Mathan[#], Anuradha Singh[#], Vikram Jathar[#], Aashish Ranjan*
National Institute of Plant Genome Research, Aruna Asaf Ali Marg, New Delhi-110067, India.
[#]These authors contributed equally to the work.

***Corresponding Author**
email: aranjan@nipgr.ac.in
Phone no. 91-11-26735117

Authors' email
Jyotirmaya Mathan: jyotirmaya@nipgr.ac.in
Anuradha Singh: annusingh1206@gmail.com
Vikram Jathar: vikram204@nipgr.ac.in

Date of submission: 22nd November 2020

Number of figures and tables: 6 figures and 3 tables

The word count: 5,453

Supplementary data: 6 supplemental figures and 7 supplemental tables

Title: Rubisco activity, electron transport rate, and leaf features drive high photosynthesis rate in the selected wild rice

Running Head: Efficient photosynthesis in the selected wild rice

Highlight

Distinct leaf biochemical, photochemical, and developmental features contribute to efficient photosynthesis in the selected wild rice that could potentially be exploited for increasing rice leaf photosynthesis.

Abstract

The importance of increasing photosynthetic efficiency for sustainable crop yield increases to feed the growing world population is well recognized. The natural genetic variation for leaf photosynthesis in crop plants is largely unexploited for increasing genetic yield potential. The genus *Oryza*, including cultivated rice and wild relatives, offers tremendous genetic variability to explore photosynthetic differences, and underlying biochemical, photochemical, and developmental basis. We quantified leaf photosynthesis and related physiological parameters for six cultivated and three wild rice genotypes, and identified photosynthetically efficient wild rice species. Fitting A/C_i curves followed by experimental validation showed that the leaf photosynthesis in cultivated rice varieties, IR64 and Nipponbare, was limited due to Rubisco activity and electron transport rate, compared to photosynthetically efficient wild rice species, *Oryza australiensis* and *Oryza latifolia*. The selected wild rice species with high leaf photosynthesis per unit area had striking anatomical features, such as larger mesophyll cells with more chloroplasts, larger and closer veins, and fewer mesophyll cells between two consecutive veins. Our results show the existence of desirable variations in Rubisco activity, electron transport rate, and mesophyll and vein features in the rice system itself that could possibly be targeted for increasing the photosynthetic efficiency of cultivated rice varieties.

Keywords: A/C_i curve, Chlorophyll fluorescence, Electron transport rate, Leaf anatomy, Photosynthesis, Photosystem II (PSII), Rubisco activity, Wild rice.

Introduction

A remarkable increase in food grain production is needed to meet the demand of the growing world population that is expected to reach 10 billion by 2050 (Alexandratos and Bruinsma, 2012). Crop yield increases due to extensive breeding and agronomic practices are approaching a plateau over the last decade (Peng *et al*., 2008; Lawson *et al*., 2012). Increasing photosynthetic efficiency of crop plants could be an important strategy for further increases in crop yield potential and productivity (Zhu *et al*., 2010; Lawson *et al*., 2012; Ort *et al*., 2015; Simkin *et al*., 2019). There have been examples of increases in photosynthetic efficiency in crop plants. Specific developmental and biochemical features are known to promote efficient photoassimilation of CO_2 in C_4 plants (Kajala *et al*., 2011; Koteyeva *et al*., 2011). The potential of increasing photosynthetic efficiency to improve yield potential in C_3 plants has been shown by Free-air CO_2 enrichment (FACE) experiments (Rogers *et al*., 2004; Rosenthal *et al*., 2012; Kimball, 2016).

Photosynthesis, the key biochemical process fixing atmospheric CO_2 in the form of carbohydrates, is a multifaceted process that has contributions from leaf physiological, biochemical, and developmental features (Long *et al*., 2006; Mathan *et al*., 2016). Over the past years, the biochemical understanding of photosynthesis has been extensively elaborated. The studies have highlighted the potential biochemical targets, such as decreasing Rubisco oxygenase activity, increasing RuBP regeneration, suppressing photorespiration, and increasing photoprotection of the photosynthesis, that could be optimized to improve photosynthetic efficiency (Long *et al*., 2006; Murchie and Niyogi, 2011). The response of net CO_2 assimilation under saturating light to intercellular CO_2 concentrations (A/C_i curve) is extensively used to deduce biochemical limitations to efficient leaf photosynthesis (Long and Bernacchi, 2003; Sharkey *et al.*, 2007). The Farquhar–von Caemmerer–Berry (FvCB) model along with its later extension described *in vivo* Rubisco activity (V_{cmax}), maximum electron transport rate (J_{max}) determining the regeneration of ribulose phosphate (RuBP) for Rubisco, and the maximum rate of triose phosphate utilization (*TPU*) as the three major biochemical limitations to leaf photosynthesis (Farquhar *et al.*, 1980; Sharkey, 1985; von Caemmerer, 2000). The genotypic variations for these biochemical limitations across landraces and accessions of crop plants have been attributed to photosynthetic differences. For example, Acevedo-Siaca *et al.* (2020) recently investigated the variation among rice accessions to show V_{cmax} as the primary limitation to photosynthetic induction. Therefore, identification of the biochemical limitations for different genotypes will not only provide insights into photosynthesis physiology under different environmental conditions but also potential ways to

105 improve crop photosynthetic efficiency by overcoming these limitations (Kromdijk *et al.*,
106 2016; Simkin *et al.*, 2019; South *et al.*, 2019; De Souza *et al.*, 2020).
107 Leaf photosynthesis limitation due to Rubisco activity, which primarily occurs at low
108 intercellular CO_2 concentration (< 200 μmol mol^{-1}), is due to the low activity of Rubisco along
109 with competing carboxylation and oxygenation reactions mediated by the enzyme (von
110 Caemmerer, 2000; Parry *et al.*, 2007; Sharkey *et al.*, 2007). Exploration and utilization of
111 efficient natural variants of Rubisco as well as engineering Rubisco have been suggested as
112 possible strategies to address this limitation of photosynthesis (Parry *et al.*, 2007; Parry *et al.*,
113 2013; Lin *et al.*, 2014; Sharwood, 2017). In addition, developmental and metabolic features
114 mediating increased concentration of CO_2 and RuBP at the active site of Rubisco could also
115 overcome the limitation. Organization of LHCs, the quantum efficiency of the photosystem,
116 and photochemical and non-photochemical quenching are key factors for determining
117 photosynthetic limitation due to electron transport rate and RuBP regeneration that operates at
118 CO_2 concentration > 300 μmol mol^{-1} (Murchie and Lawson, 2013; Wu *et al.*, 2019).
119 Approaches to increase light harvesting by PSII reaction centers and photochemical quenching,
120 which are evaluated using chlorophyll fluorescence quantification, could possibly be effective
121 in increasing leaf photosynthesis per unit area by overcoming the limitation due to electron
122 transport rate (Kalaji *et al.*, 2016; Cardona *et al.*, 2018). *TPU* drives sucrose synthesis from
123 primary photosynthates, and *TPU*-limited photosynthesis primarily operates at high CO_2
124 concentrations that often determines A_{max} (Fabre *et al.*, 2019; Sharkey *et al.*, 2007).
125 In addition to the biochemical limitations, stomatal conductance (g_S) and mesophyll
126 conductance (g_m) that affect leaf gaseous exchange are critical determinants of leaf
127 photosynthesis (Farquhar and Sharkey, 1982). Extrinsic factors, such as light intensity and CO_2
128 concentration, influence photosynthetic performance by regulating the activity of light-
129 harvesting complexes (LHCs), Rubisco, and opening/closing of stomata (Eichelmann and
130 Laisk, 2002; Murchie and Niyogi, 2011; Hiyama *et al.*, 2017). Developmental characteristics
131 of leaves are also strong determinants of photosynthesis (Mathan *et al.*, 2016). Flag leaf width
132 (FLW), flag leaf thickness (FLT), and specific leaf area showed a positive correlation with
133 photosynthetic capacity, thus affecting overall crop performance (Liu *et al.*, 2015). Anatomical
134 features such as size, lobbing, and surface area of mesophyll cells are critical for proper light
135 distribution and CO_2 diffusion within a leaf (Flexas *et al.*, 2008; Sage and Sage, 2009; Tholen
136 *et al.*, 2012). Similarly, vein density and interveinal distance have been shown to influence CO_2
137 fixation efficiency (Amiard *et al.*, 2005; Brodribb *et al.*, 2007). Thus, investigating

138 relationships between leaf anatomy and photosynthetic features could help in optimizing crop
139 photosynthetic efficiency (Evans, 2013).
140 The genotypic variations for leaf photosynthesis, and underlying biochemical,
141 photochemical, and developmental attributes, are largely unexploited resources for crop
142 improvement (Flood *et al*., 2011; van Bezouw *et al*., 2019). Rice, with two cultivated species:
143 *Oryza sativa* (Asian rice with two subspecies: *indica* and *japonica*) and *Oryza glaberrima*
144 (African rice), and many related wild rice species, provides an excellent system to investigate
145 photosynthetic differences and underlying genetic basis. A comprehensive phylogenetic
146 relationship for the genus *Oryza*, including all the species and genome types, was inferred by
147 Sanchez *et al.* (2013). A recent study has detailed the molecular evolution in the genus *Oryza*,
148 and showed the complex evolution of two domesticated species, *Oryza sativa* and *Oryza*
149 *glaberrima*, that involved introgressions among different chromosomes (Stein *et al*., 2018).
150 We examined a set of cultivated (including both subspecies of *Oryza sativa* and African
151 cultivated rice *Oryza glaberrima*) and wild rice species (*O. rufipogon*, *O. latifolia*, and *O.*
152 *australiensis*) to find out photosynthetically efficient wild relatives of rice. We, then, identified
153 the biochemical limitations, Rubisco activity and maximum electron transport rate, to leaf
154 photosynthesis in the cultivated varieties compared to the selected wild species. Photochemical
155 and developmental differences, further, corroborated the leaf photosynthesis differences across
156 the selected cultivated and wild rice.
157
158 **Materials and methods**
159 **Plant material and growth conditions**
160 Nine rice genotypes, consisting of four varieties of *Oryza sativa* ssp. *indica* (IR 64, Swarna,
161 Nagina 22, and Vandana), a variety of *Oryza sativa* ssp. *japonica* (Nipponbare), African
162 cultivated rice *Oryza glaberrima*, and three wild rice species, *Oryza rufipogon*, *Oryza latifolia*,
163 and *Oryza australiensis* were grown at research field of National Institute of Plant Genome
164 Research, New Delhi (average air temperature > 25 °C, 70-80% humidity, and more than 100
165 cm annual rainfall) (Supplementary Table S1). These genotypes were also grown under
166 controlled growth chambers in round pots (15 cm diameter × 14 cm height; one plant per pot),
167 and were supplied with Hoagland solution weekly. The growth conditions were maintained as
168 28/22ºC day and night air temperature, 70-80% relative humidity, a photoperiodic cycle of
169 14h:10h (light:dark), and 1500 µmol m^{-2} s^{-1} light intensity. Five biological replicates
170 (individual plants) of each genotype were grown in randomized complete block design and re-
171 randomized every 7th day to control the confounder within controlled growth chambers.

172

173 **Photosynthesis rate and related physiological trait measurements**

174 Both field-grown plants, as well as chamber-grown plants, were used for detailed
175 quantification of photosynthesis rate and related physiological traits. Leaf photosynthesis of
176 field-grown plants was measured at ten days after heading from the middle widest part of fully
177 expanded flag leaves using LI-6400XT portable photosynthesis system using 2 × 3 cm standard
178 leaf chamber (LI-6400, LI-COR, Inc). For the accessions with leaf width less than 2 cm, the
179 leaf chamber was filled using two flag leaves carefully without any overlap (Busch, 2018). For
180 all measurements, the leaf chamber was maintained at ambient atmospheric CO_2 concentration
181 (*Ca*, 400 µmol mol^{-1}), natural light irradiance, constant airflow (300 µmol s^{-1}), 70-80% relative
182 humidity, leaf and air temperature (28-30ºC), and leaf-to-air maximum vapor pressure deficit
183 in the range of 1.0-1.5 kPa. Gas exchange measurements were performed between 9.00 h to
184 11.00 h on clear sunny days. Fifteen flag leaves from different plants were used to quantify net
185 photosynthesis rate (*A*), intercellular CO_2 concentration (C_i), stomatal conductance to water
186 (g_s), and carboxylation efficiency (*CE*, the ratio of *A* to C_i). Values were recorded when *A*, g_s,
187 and C_i became stable.

188 *A*, g_s, C_i and *CE* were also quantified from the widest part of fully-grown eight leaves
189 of chamber-grown plants using a 2 cm^2 leaf chamber with a LED light source (LI-6400-02B;
190 LI-COR, Inc). Leaf chamber was maintained at 1000 µmol m^{-2} s^{-1} light intensity, 400 µmol
191 mol^{-1} CO_2 concentration, 300 µmol s^{-1} constant airflow, 70-80% relative humidity, leaf and air
192 temperature of 28 and 30 ºC, respectively, and leaf-to-air maximum vapor pressure deficit in
193 the range of 1.0-1.5 kPa.

194

195 **Estimation of leaf chlorophyll content**

196 Total chlorophyll content (*TCC*) was measured in aqueous 80% acetone following the
197 procedure described in Porra *et al.* (1989). Briefly, flag leaves (2.0 × 1.0 cm) of field-grown
198 plants and fully-grown eighth leaves of chamber-grown plants (five biological replicates per
199 genotypes) were harvested and incubated in 5 ml of ice-cold 80% acetone for 48 h, centrifuged
200 at 5,000 × g for 5 min, and absorbance was recorded at 663 nm (Chl a) and 645 nm (Chl b).
201 The pigment concentration (Chl a + b) was calculated using the method described by Arnon,
202 (1949) and expressed in µmol m^{-2}.

203

204 **Quantification of leaf photosynthesis (*A*) and stomatal conductance (g_s) at different light**
205 **intensities**
206 Plants grown under controlled growth conditions were used to examine the effect of light
207 intensity on *A* and g_s. The measurements were performed on the middle widest part of fully-
208 grown eighth leaves of chamber-grown plants (five biological replicates per genotypes) using
209 2 cm^2 standard leaf chamber with a LED light source (LI-6400-02B; LI-COR, Inc). The leaf
210 chamber was maintained at a constant temperature and relative humidity for all measurements
211 as explained above. The CO_2 concentration (C_a) was set at 400 µmol mol^{-1}. Leaves were
212 initially stabilized at the highest irradiance (i.e. 2000 µmol m^{-2} s^{-1}), and then PPFD was
213 gradually decreased in a step-wise manner (1800, 1500, 1200, 1000, 700, 500, 300, 100 µmol
214 m^{-2} s^{-1}). Data were recorded at each point once *A* and g_s values were stable.
215
216 **Quantification of *A*, g_s, and chlorophyll fluorescence at different CO_2 concentrations**
217 The effect of varying CO_2 concentration on *A* and g_s, as well as on leaf chlorophyll
218 fluorescence, was quantified simultaneously using plants grown under controlled growth
219 conditions. Values were recorded from the middle widest part of fully-grown eighth leaves of
220 chamber-grown plants (five biological replicates per genotypes) under 1500 µmol m^{-2} s^{-1} light
221 conditions intensity using 2 cm^2 standard leaf chamber fluorometer (LI-6400-40 LI-COR, Inc)
222 according to the method described in Li *et al*. (2009) and Fabre *et al*. (2019). Before
223 measurements, leaves were stabilized at ambient CO_2 concentration (400 µmol mol^{-1}) and
224 saturating light intensity for at least 10 minutes. The concentration of CO_2 in the leaf chamber
225 (C_a) was decreased from 400 µmol mol^{-1} concentration to 300, 200, 150, 100, 80, µmol mol^{-1}
226 CO_2, and then increased in a step-wise manner to 400, 600, 800, 1000, 1200, and 1400 µmol
227 mol^{-1} CO_2. CO_2 and H_2O diffusion through the gasket was corrected according to the
228 manufacturer's instructions (LI-COR 6400XT manual version 6). The leaf and air temperature,
229 relative humidity, airflow, and vapor pressure deficit were maintained as mentioned above.
230 For photochemical traits, steady-state fluorescence (F_s) was quantified at different CO_2
231 concentrations. Light-adapted maximum fluorescence (F_m') was determined at each CO_2
232 concentration by illuminating 2.0 cm^2 leaf surface inside the chamber with a saturated pulse of
233 light (about 8000 µmol m^{-2} s^{-1} for 0.8 sec), provided by an array of light-emitting diodes (a
234 mixture of 90% red and 10% blue lights at 640 and 460 nm peak wavelength, respectively).
235 Minimal fluorescence level in the light-adapted state (F_o') was determined after removal of the
236 actinic light, and illuminating the leaf with 1 sec of far-red light (735 nm). Using F_s, F_m' and
237 F_o', we calculated (a) the efficiency of PSII ($\phi PSII$) (b) the coefficient of photochemical

quenching (qP), and (c) the photosynthetic electron transport rate (J_{PSII}) in a light-adapted state using following formulae as described in Murchie and Lawson, (2013).

$$\phi PSII = (F_m' - F_s)/ F_m'$$

$$qP = (F_m' - F_s)/ (F_m' - F_o')$$

$$J_{PSII} = \alpha \times \beta \times \phi PSII \times \text{PPFD}$$

where PPFD is incident photosynthetic photon flux density (i.e., 1500 μmol m^{-2} s^{-1}), β is the photosystem partitioning factor between PSI and PSII for the distribution of light (0.5), and α is the leaf absorbance calculated from total chlorophyll content per unit leaf area (*TCC*, μmol m^{-2}) for each rice genotype. *TCC* was quantified from fully grown leaves of growth-chamber grown plants at the same stage when photosynthesis was measured (Supplementary Table S2). α was calculated from *TCC* using the following formula as described in Evans and Poorter, (2001):

$$\alpha = [TCC]/([TCC] + 76)$$

Quantification of mitochondrial respiration rate in the light (R_d) and the CO_2 compensation point related to C_i (Γ*)

R_d and Γ* were quantified at the intersection point of multiple A/C_i response curves, conducted at a series of CO_2 concentrations and multiple light intensities using plants grown under controlled growth conditions (Laisk, 1977; Li *et al.*, 2009). *A* was recorded from the middle (widest) part of fully-grown eighth leaves of chamber-grown plants using 2 cm^2 standard leaf chamber fluorometer (LI-6400-40 LI-COR, Inc). Light intensity inside the leaf chamber was controlled as a series of 100, 200, and 500 μmol m^{-2} s^{-1}. At each light intensity, CO_2 concentration was adjusted in the series of 75, 100, 125, and 150 μmol mol^{-1} inside the chamber. The leaf and air temperature, relative humidity, airflow, and vapor pressure deficit were maintained as explained above. CO_2 and H_2O diffusion through the gasket was corrected according to the manufacturer's instructions (LI-COR 6400XT manual version 6). The value of *A* at the point of intersection of the three A/C_i curves represented $-R_d$, and C_i at the point represented Γ*(Li *et al.*, 2009).

Quantification of mesophyll conductance (g_m)

Mesophyll conductance (g_m) at ambient CO_2 concentration (400 μmol mol^{-1}) was quantified using the formula $g_m = A/(C_i - C_c)$, where C_c is the chloroplastic CO_2 concentration. C_c was calculated according to the variable J method (Harley *et al.*, 1992) as:

$$C_c = \frac{\Gamma * \times [J+8(A+R_d)]}{J-4(A+R_d)}$$

where Γ* is CO_2 compensation point (μmol mol^{-1}), R_d is mitochondrial respiration rate in the light (μmol m^{-2} s^{-1}), and J is the rate of photosynthetic electron transport, which was estimated using chlorophyll fluorescence analysis as J_{PSII} (described above). Genotype-specific values of variables were used for the calculation of g_m for each genotype.

Fitting the FvCB model to estimate biochemical limitations

We used the non-linear fitting method explained by Sharkey (2016), version 2 to fit the FvCB model. Three major photosynthetic limitations, the maximum velocity of Rubisco carboxylation (V_{cmax}), maximum electron transport rate for RuBP regeneration (J_{max}), and maximum rate of triose phosphate utilization (*TPU*) were estimated simultaneously by minimizing the sum of squares of the residuals. Genotype-specific values of g_m, R_d, and Γ* (as explained above) were used for fitting the model. Rice Rubisco catalytic constants were taken from Perdomo *et al.* (2017). All parameters were scaled to a constant temperature of 25ºC. Before fitting the curves, values for each curve were corrected for diffusive leaks between the cuvette and the external environment (Bernacchi *et al.*, 2001). Rubisco limitation (A_c), RuBP-regeneration limitation (A_j), and TPU limitation (A_t) to photosynthesis for different accessions were estimated using the following formulae:

$$A_c = V_{cmax}\left[\frac{C_c - \Gamma^*}{C_c + K_c\,(1+\frac{O}{K_O})}\right] - R_d$$

$$A_j = J_{max}\frac{C_c - \Gamma^*}{4C_c + 8\Gamma^*} - R_d$$

$$A_t = 3TPU - R_d$$

where O is partial pressure for oxygen, and K_C and K_O are Rubisco catalytic constants.

Rubisco activity assay

Rubisco activity assay was performed following the procedure described in Kubien *et al.* (2011) and Sharwood *et al.* (2016a). Briefly, illuminated leaf tissues (3.6 × 1.0 cm) were excised from the middle widest part of flag leaves of the field-grown plant (one leaf per plant, three different plants per genotype) between 9.00 h to 10.00 h and homogenized in extraction buffer [EB, 5 mM DTT, 10 mg ml^{-1} PVPP, 2 mg ml^{-1} BSA, 2 mg ml^{-1} PEG, 2% (v/v) Tween-80, 12 mM 6-aminocaproic acid, 2.4 mM benzamidine in HEPES stock) at 4 ºC. The

304 homogenate was centrifuged for 1 min at ~16,000 × *g* and the pellet was discarded. To activate
305 rubisco enzyme, leaf extracts were incubated with BMEC (100 mM Bicine-NaOH, pH 8.2, 20
306 mM $MgCl_2$, 1 mM Na_2-EDTA and 10 mM $NaHCO_3$) in a 9:1 ratio (e.g. 900 µL leaf extract to
307 100 µL BMEC) at 25 ºC for 25 min. To assess the activity of Rubisco from leaf extract, 50 µl
308 of leaf extract was incubated with 1,550 ml of the EME buffer, 40 µl 10 mM of NADH (final
309 concentration 200 µM), 80 µl of 250 mM $NaH^{12}CO_3$ (10 mM), 200 µl of ATP/phosphocreatine
310 (1 and 5 mM, respectively), 40 µl of coupling enzymes (Carbonic anhydrase 500U,
311 Glyceraldehyde-3-P dehydrogenase 50U, 3-PGA kinase 50U, Triose-P Isomerase/Glycerol-3-
312 P dehydrogenase 400/40U), 40 µl of 25 mM RuBP (500 µM), mixed gently, and decrease of
313 absorbance were monitored at 340 nm continuously for 0 to 1800 sec using a UV–Vis
314 spectrophotometer. The Rubisco carboxylation rate was determined using the equation:

315 $$RuBP - use\ (\mu mol\ s^{-1}) = \frac{\Delta \mathrm{OD}_{340} * \mathrm{Vol}}{6.18\ \mathrm{X}\ 4}$$

316 assuming an extinction coefficient of 6.18 µmol ml^{-1} cm^{-1} for NADH oxidation at 340 nm.
317 ΔOD_{340} is the rate of change of absorbance at 340 nm per second, and Vol is assay volume (1
318 ml). The equation accounts for the four NADH molecules oxidized per RuBP carboxylated by
319 Rubisco.
320 The activity of Rubisco (V_{cmax}) is calculated as:
321

322 $$V_{cmax}\left(\mu mol^{-m^2 s}\right) = \frac{(RuBP - use;\ \mu mol\ s^{-1})(EV;\ \mu l)(10000\ cm^2/m^2)}{(LA; cm^2)\ (Sample\ volume;\ \mu l)}$$

323 where EV is extraction volume and LA is leaf area.
324

325 **RNA isolation and expression analysis**

326 Total RNA was isolated from flag leaves in three biological replicates for each genotype, and
327 each biological replicate consisted of tissues from multiple individual plants. Tissues were
328 harvested and immediately frozen in liquid nitrogen. Total RNA extraction (TRIzol reagent),
329 DNase treatment, and cDNA synthesis (RevertAid First-strand cDNA synthesis kit) were
330 performed according to the manufacturer protocol (Thermo Fisher Scientific). The PowerUp™
331 SYBR® Green fluorescence dye was used for quantitative gene expression analysis on CFX
332 connect Real-time PCR detection system (Bio-Rad). The details of genes used for expression
333 analysis and the primers are presented in Supplementary Table S3 and S4. The specificity of
334 amplified gene products across the selected rice genotypes using the listed primers was viewed
335 through dissociation curve analysis. Before quantitative real-time PCR, the efficiency of each

336 primers pair was evaluated using a standard curve method where four cDNA quantities (1, 10,
337 50, and 100 ng) from one of the cultivated rice (Nipponbare) was used to construct a standard
338 curve, and efficiency was calculated for each genotype using the formula $E = (10^{[-1/slope]}-$
339 $1)*100$. Expression analysis of each gene was performed in three biological replicates for each
340 genotype, and repeated twice for the reproducibility of the results. Rice actin
341 (LOC_Os03g50885.1) was used as an internal control gene for the normalization of gene
342 expression. The relative change was calculated following the method of Livak and Schmittgen
343 (2001).
344
345 **Visualization and quantification of leaf developmental traits**
346 The widest middle part of the flag leaves of 10 -15 field-grown plants was used to measure flag
347 leaf width (FLW) and leaf thickness (FLT). For anatomical traits visualization, transverse
348 sections were cut from the mid-portion of flag leaves (one leaf per plant, five biological
349 replicates per genotype), and stained with toluidine blue with some modification of the method
350 as described in Lux *et al.* (2005). Briefly, chlorophyll pigments of the thin sections were cleared
351 using 85 % (w/v) lactic acid saturated with chloral hydrate, heated on a water bath at 70 ºC for
352 1 h, and washed several times with distilled water. To visualize mesophyll cells, sections were
353 incubated in absolute alcohol overnight and stained with 1% toluidine blue in 1% (w/v)
354 disodium tetraborate for 15 sec. Finally, thin sections were mounted with 50 % glycerol and
355 visualized using a bright field microscope (LMI, UK). The quantification of leaf anatomical
356 features related to the minor vein, mesophyll cell and, bundle sheath cells were performed at
357 10X and 100X magnification (four images per leaf, two on each side of the midrib that
358 consisted of about 3-6 complete cells per image) using Fiji-Image J software (Wayne Rasband,
359 National Institute of Health) as described in Chatterjee *et al.* (2016) and Ivanova *et al.* (2018).
360
361 **Chloroplast ultrastructure**
362 Freshly harvested flag leaf segments (1 × 1 mm; one leaf each from three individual plants per
363 genotype) were fixed under buffer (3% glutaraldehyde in 0.1 M cacodylate buffer, pH 7.2) for
364 2 h, and then treated with 1% osmium tetroxide overnight at 4 ºC. The fixed segments were
365 dehydrated in a graded acetone series and embedded in epoxy resin. Ultrathin sections were
366 cut with diamond knives, stained with uranyl acetate and lead citrate double staining procedure
367 as described by Reynolds, (1963). Chloroplasts of the uppermost part of the leaf sections were
368 viewed using a digital camera (BH-2, Olympus) equipped with transmission electron
369 microscopy at 1000X magnification (JEM 1230; JEOL).

370

371 **Statistical analysis**

372 Differences among the genotypes were tested by one-way analysis of variance (ANOVA) (JMP
373 Pro, version 12.0.1; SAS Institute, Cary, NC, USA). Statistically similar genotypes were
374 grouped according to post-hoc Tukey HSD calculation. Significance test for the genotypes at
375 varying light intensities and CO_2 concentrations, as well as for Rubisco activity differences
376 was performed using one-way Analysis of Variance (ANOVA). Pearson correlation matrix was
377 calculated based on mean values of each trait for each genotype to evaluate the trait-to-trait
378 associations. The threshold for statistical significance was $P \leq 0.05$. Linear regression analyses
379 between V_{cmax}/J_{max}, V_{cmax}/TPU, and J_{max}/TPU were performed using Microsoft Excel.

380

381

382 **Results**

383 **Quantification of leaf photosynthesis and related physiological features**

384 We observed remarkable differences for leaf photosynthesis (*A*) and related
385 physiological features among the selected cultivated and wild rice accessions (Fig. 1). The
386 mean *A* value for the wild rice species, *O. latifolia*, *O. australiensis*, and *O. rufipogon*, and
387 African cultivated rice *O. glaberrima* were found to be significantly higher than that of
388 cultivated rice varieties, such as IR64, Nagina 22, and Vandana (Fig. 1A). Among the selected
389 accessions, *O. australiensis* and *O. latifolia* showed the highest *A*, 23.50 and 24.18 μmol CO_2
390 m^{-2} s^{-1}, respectively. Also, we observed significant variations for *A* among the cultivated
391 varieties. For instance, one of the high-yielding *indica* variety Swarna and *japonica* variety
392 Nipponbare displayed higher *A* compared to other cultivated varieties (Fig. 1A).

393 We further examined important physiological traits, known to influence leaf
394 photosynthesis, of the selected accessions. As expected, wild rice species, *O. latifolia* and *O.*
395 *australiensis* with highest *A*, showed higher stomatal conductance (g_s), and intercellular CO_2
396 concentration (C_i) (Fig. 1B, C). In addition, these species along with *O. rufipogon* displayed
397 higher carboxylation efficiency (*CE*) than those of cultivated rice (Fig. 1D). Among the
398 cultivated varieties, Nipponbare that displayed higher *A* also showed reasonably higher g_s and
399 *Ci* compared to other cultivated varieties. We also observed the strong differences in total
400 chlorophyll content (*TCC*) in flag leaves of the selected accession. Consistent with the high *A*,
401 wild species *O. latifolia*, *O. australiensis*, and *O. rufipogon* had higher *TCC* per unit leaf area
402 compared to the cultivated varieties. *O. glaberrima*, Swarna, and Nipponbare also had
403 reasonably higher *TCC* than IR 64, Nagina 22, and Vandana (Fig. 1E). Pearson correlation

404 analysis showed a significant positive correlation of A with g_s ($r = 0.629$), C_i ($r = 0.570$), CE
405 ($r = 0.819$), and TCC ($r = 0.912$), g_s with C_i ($r = 0.965$) and CE with TCC ($r = 0.906$) at $P \leq$
406 0.05 (Supplementary Fig. S1).
407 We further quantified leaf photosynthesis and related physiological traits for fully-
408 grown eight leaves of plants grown under controlled conditions. Similar to our observations at
409 the full heading stage under field conditions, wild rice species together with African cultivated
410 rice *O. glaberrima* showed significantly higher A, g_s, and CE compared to cultivated rice since
411 the beginning of the vegetative stage (Supplementary Table S5). Taken together, these results
412 showed significant differences in photosynthetic traits across the set of cultivated and wild rice.
413 We then, selected representative cultivated rice accessions (*O. sativa* ssp. *indica* cv. IR 64, *O.*
414 *sativa* ssp. *japonica* cv. Nipponbare, and African cultivated rice *O. glaberrima*) and wild rice
415 species (*O. latifolia* and *O. australiensis)*, which captured the entire variation range in the
416 experiment for the leaf photosynthesis per unit area, for detailed analyses (Fig. 1F;
417 Supplementary Fig. S2).
418
419 **Effect of varying light intensity and CO_2 concentration on leaf photosynthesis and**
420 **stomatal conductance**
421 Light intensity and CO_2 concentration are the two most important factors determining
422 leaf photosynthesis. Therefore, we examined the effect of different light intensity and CO_2
423 concentration on A and g_s of the selected wild and cultivated rice accessions grown under
424 controlled conditions (Fig. 2). All the selected species showed a steeper initial slope,
425 instantaneous enhancement followed by a plateau for leaf photosynthesis per unit area to
426 achieve maximum A (A_{max}) with the increase in photosynthetic photon flux density (PPFD) and
427 CO_2 concentration (Fig. 2A and 2C). Wild rice species, *O. latifolia* and *O. australiensis*,
428 exhibited higher increases in A in response to increasing PPFD compared to cultivated varieties
429 (Fig. 2A). *O. latifolia* and *O. australiensis* had significantly higher $A_{max,}$ 20.94 and 21.68 µmol
430 CO_2 m^{-2} s^{-1}, respectively, at 1800 µmol m^{-2} s^{-1} PPFD compared to *O. sativa* cv. IR 64 and *O.*
431 *sativa* cv. Nipponbare (11.89 and 13.02 µmol CO_2 m^{-2} s^{-1}, respectively). The selected wild rice
432 species were also able to maintain higher g_S, compared to cultivated varieties at different light
433 intensities (Fig. 2B)
434 The effect of increasing CO_2 concentration on A segregated the selected genotypes
435 under three distinct groups: *O. australiensis* and *O. latifolia* with higher A, African cultivated
436 rice *O. glaberrima* with intermediate A, and cultivated varieties Nipponbare and IR 64 with
437 lower A at different CO_2 concentration (Fig. 2C). A sharp increase in A was observed with

438 increasing CO_2 concentration up to 1000 µmol mol^{-1}, followed by saturation for all the
439 accessions. The extent of increase in *A* was less in cultivated varieties, IR 64 and Nipponbare,
440 compared to African cultivated rice *O. glaberrima*, and wild rice *O. australiensis* and *O.*
441 *latifolia* (Fig. 2C). The g_s, however, showed a decreasing trend at increasing CO_2
442 concentration, likely due to the closure of stomata (Fig. 2D). Altogether, the selected wild rice
443 species, *O. australiensis* and *O. latifolia*, were able to maintain higher photosynthesis per unit
444 area at different light intensities and CO_2 concentrations compared to the selected cultivated
445 varieties.
446
447 **Fitting CO_2 response curves to investigate biochemical limitations V_{cmax}, J_{max}, and *TPU***
448 To investigate the biochemical limitations to photosynthesis across the selected
449 accessions using the FvCB model, we first estimated mesophyll conductance (g_m) at ambient
450 CO_2 concentration. g_m significantly varied for the selected cultivated and wild rice species
451 (Table 1). *O. australiensis* and *O. latifolia*, with highest *A*, also showed higher g_m compared to
452 the cultivated varieties, suggesting the key importance of g_m for photosynthetic variations
453 among the genotypes. We also quantified the mitochondrial respiration rate in the light (R_d)
454 and CO_2 compensation point related to C_i (Γ^*) for each genotype to fit the FvCB model (Table
455 1). R_d was found to be significantly higher for *O. australiensis* and *O. latifolia* compared to the
456 selected cultivated accessions, whereas no significant difference was observed for Γ^* across
457 the accessions.
458 We, then, used carbon dioxide response (A/C_i) curves to estimate maxima of Rubisco
459 carboxylation activity (V_{cmax}), regeneration of ribulose-1,5-biphosphate expressed as electron
460 transport rate (J_{max}), and triose phosphate utilization (*TPU*) for the selected accessions
461 (Farquhar *et al*., 1980; von Caemmerer, 2000). A_{max} for the selected accessions ranged from
462 20.07 µmol CO_2 m^{-2} s^{-1} for cultivated variety IR 64 to 36.81 µmol CO_2 m^{-2} s^{-1} for the wild
463 species *O. australiensis* (Table 2). We found significantly higher values V_{cmax}, J_{max}, and *TPU*
464 for the wild species *O. australiensis* and *O. latifolia* compared to cultivated varieties IR64 and
465 Nipponbare, suggesting V_{cmax}, J_{max}, and *TPU* together might contribute to differences in A_{max}.
466 Consistent with the intermediate value of A_{max} for *O. glaberrima*, the values of biochemical
467 limitations were also intermediate between the wild species and cultivated *indica* and *japonica*
468 varieties. We investigated the relationship among the modeled biochemical limitations to
469 photosynthesis across the selected accessions. A distinct linear relationship was observed
470 between V_{cmax} and J_{max} (R^2 = 0.973), J_{max} and *TPU* (R^2 = 0.987), and V_{cmax} and *TPU* (R^2 =
471 0.968) at $P < 0.001$, suggesting the robustness of the modelled limitations (Supplementary Fig.

472 S3). These results, expectedly, indicated the important contribution of biochemical attributes
473 to photosynthetic differences among the selected cultivated and wild rice accessions.
474 We, then, calculated the photosynthetic limitations due to V_{cmax} (A_c), J_{max} (A_j), and *TPU*
475 (A_t). Generally, Rubisco-limited photosynthesis (A_c) occurs at CO_2 concentration < 200 µmol
476 mol^{-1}, while RuBP-regeneration limits photosynthesis (A_j) at CO_2 concentration > 300 µmol
477 mol^{-1}. Limitation to photosynthesis beyond A_j, at high CO_2 concentrations, is attributed to A_t
478 which often determines A_{max} (Sharkey *et al*., 2007; Fabre *et al*., 2019). The transition from
479 Rubisco-limited (A_c) to RuBP-regeneration limited (A_j) photosynthesis in Asian cultivated rice,
480 IR 64 and Nipponbare, was observed at C_i < 250 µmol mol^{-1} (Supplementary Table S6). In
481 contrast, wild rice species *O. australiensis* and *O. latifolia* along with African cultivated rice
482 *O. glaberrima* showed A_c to A_j transition at C_i > 300 µmol mol^{-1}. Similarly, the transition from
483 RuBP-regeneration limited (A_j) to TPU-limited (A_t) photosynthesis in Nipponbare and IR 64
484 was observed at C_i 524 and 608 µmol mol^{-1}, respectively, which was lesser compared to *O.*
485 *glaberrima* (657 µmol mol^{-1}), *O. australiensis* (700 µmol mol^{-1}), and *O. latifolia* (713 µmol
486 mol^{-1}) (Supplementary Table S6). A_{max} that ranged from 20.07 µmol CO_2 m^{-2} s^{-1} in IR 64 to
487 36.81 µmol CO_2 m^{-2} s^{-1} in *O. australiensis*, further, indicated TPU-limitation (A_t) in IR64 and
488 Nipponbare compared to the wild rice species. However, the TPU-limitation is observed at C_i
489 much higher than the physiological conditions as reported earlier (Kumarathunge *et al*., 2019).
490 These results suggested that leaf photosynthesis per unit area in Asian cultivated varieties, IR
491 64 and Nipponbare, was limited due to Rubisco activity (V_{cmax}) and RuBP-
492 regeneration/Electron Transport Rate (J_{max}) compared to the selected wild rice genotypes under
493 ambient CO_2 concentrations.
494
495 **Photochemical differences among the selected rice accessions**
496 Since the estimation of biochemical limitations to photosynthetic differences across the
497 selected accessions suggested J_{max} as one of the limiting factors, we used leaf chlorophyll
498 fluorescence parameters to quantify the photochemical features of the selected rice accessions.
499 We observed strong differences in electron transport rate (J_{PSII}), the efficiency of PSII ($\phi PSII$),
500 and photochemical quenching (qP) among the selected cultivated and wild rice accessions
501 across different CO_2 concentrations, with distinct differences at CO_2 concentration higher than
502 200 µmol mol^{-1}. *O. latifolia* and *O. australiensis* showed significantly higher values of J_{PSII}
503 compared to cultivated Asian rice varieties IR 64 and Nipponbare at different CO_2
504 concentrations (Fig. 3A). Similar to J_{PSII}, values of $\phi PSII$ and qP were also significantly higher
505 for *O. latifolia* and *O. australiensis* compared to the cultivated varieties (Fig. 3B, C). *O.*

506 *glaberrima*, the African cultivated rice with reasonably higher *A*, also showed relatively higher
507 J_{PSII}, $\phi PSII$, and *qP* than *O. sativa* cultivated varieties at different CO_2 concentrations. Similar
508 response patterns of both *A* and J_{PSII} were observed at different CO_2 concentrations, and were
509 found to be strongly correlated with each other for all the selected genotypes (Supplementary
510 Fig. S4). Taken together, these results showed that photochemical features of *O. australiensis*
511 and *O. latifolia* contributed to the higher leaf photosynthesis rate, and lower J_{PSII}, $\phi PSII$, and
512 *qP* of IR 64 and Nipponbare accounted for RuBP-regeneration-limited photosynthesis in those
513 cultivated varieties.
514
515 **Rubisco activity differences across the selected rice genotypes**
516 Rubisco content as well as activity contribute considerably to differences in
517 photosynthetic activity (Parry *et al*., 2013). Moreover, our analyses on biochemical limitations
518 to photosynthesis suggested V_{cmax} as a major limitation to leaf photosynthesis per unit area in
519 the cultivated varieties IR64 and Nipponbare. Therefore, we quantified the *RuBP-use* and *in*
520 *vitro* Rubisco activity (V_{cmax}) over a period of 30 minutes across selected cultivated and wild
521 rice species (Fig. 4A, B). The CO_2-saturated *RuBP-use* gradually increased immediately from
522 10 sec to 10 min, followed by saturation for all the accessions. The *RuBP-use* was significantly
523 higher in photosynthetically efficient wild rice accessions (*O. latifolia* and *O. australiensis*)
524 than that of Asian cultivated varieties (*O. sativa* cv. IR 64, and *O. sativa* cv. Nipponbare) (Fig.
525 4A). Consistent with the *RuBP-use*, V_{cmax} was maximum for the wild rice *O. australiensis* and
526 minimum for the cultivated variety IR64 at saturation (Fig. 4B). Table 3 shows significantly
527 higher values of *RuBP-use* per sec and V_{cmax} for *O. latifolia* and *O. australiensis* compared to
528 IR 64 and Nipponbare at different time points during the assay. The results not only supported
529 the estimated photosynthetic limitations due to V_{cmax} in the selected cultivated varieties but also
530 suggested the existence of variation in Rubisco carboxylation activity per unit leaf area within
531 the rice system that could possibly be exploited for increasing CO_2 assimilation.
532
533 **Expression pattern of genes encoding core photosynthetic and chlorophyll biosynthesis**
534 **enzymes**
535 Since the differences in the Rubisco amount per unit leaf area may also contribute to
536 the Rubisco-limitation of the photosynthesis in IR 64 and Nipponbare, we checked the
537 expression pattern genes encoding Rubisco small and large subunits. In addition, we checked
538 the expression of LHC1 (Light-harvesting chlorophyll protein complex) and TPT (Triose
539 phosphate translocator) that may contribute to RuBP-regeneration- and TPU- limitations of the

540 photosynthesis, respectively (Supplementary Table S3). The expression of the selected
541 photosynthetic genes was significantly higher in *O. latifolia* and *O. australiensis* compared to
542 the selected cultivated varieties (Fig. 4C), suggesting higher photosynthesis in those species
543 could, at least in part, be due to the higher abundance of these gene products. These genes could
544 possibly increase net photosynthetic efficiency by increasing the efficiency of light capture,
545 CO_2 assimilation, and transport of triose phosphate from chloroplast to cytoplasm. Since wild
546 rice species with higher photosynthesis also showed higher chlorophyll content, we checked
547 the expression level of chlorophyll biosynthesis genes. The expression of chlorophyll
548 biosynthesis genes, such as *GluTR*, *PPOX*, *Mg-CHLD*, *CHLSYN*, and *CAO* were found to be
549 significantly higher in *O. latifolia* and *O. australiensis* compared to the selected cultivated
550 varieties (Fig. 4D).
551
552 **Leaf developmental traits underpinning photosynthetic variations**
553 Leaves are the prime photosynthetic organs, and expectedly the selected cultivated and
554 wild rice accessions exhibited considerable variation for flag leaf width (FLW) and thickness
555 (FLT) (Supplementary Fig. S5). Wild rice species had thicker and wider leaves as compared to
556 cultivated rice. Strong significant positive correlations of leaf photosynthesis were found with
557 FLW ($r = 0.850$) and FLT ($r = 0.938$) (Fig. 5A). At the anatomical level, remarkable
558 differences in the vascular architecture and mesophyll cell features were observed for the
559 selected rice accessions that differ in leaf photosynthesis (Supplementary Table S7). Wild rice
560 species with higher *A* exhibited a larger vein height and width. *O. sativa* cv. Nipponbare that
561 showed relatively higher *A* compared to other cultivated varieties also showed larger vein
562 height and width (Supplementary Table S7). Significant positive correlations were observed
563 for *A* with vein features: minor vein width (MiV-W, $r = 0.752$), minor vein height (MiV-H, r
564 $= 0.899$), and total number of veins (TV, $r = 0.848$) (Fig. 5A). Similar strong correlations of *A*
565 were observed for mesophyll cell features: mesophyll cell lobbing (M-Lo, $r = 0.760$),
566 mesophyll cell length (M-L, $r = 0.863$), mesophyll cell width (M-W, $r = 0.928$), and mesophyll
567 cell area (M-A, $r = 0.897$) at $P \leq 0.05$. However, no significant correlations of *A* and related
568 physiological traits were observed with bundle sheath features: bundle-sheath number (BS-
569 No), and bundle-sheath area (BS-A) (Fig. 5A).
570 Photosynthetically efficient wild rice species, *O. latifolia,* and *O. australiensis*, had
571 larger and closely spaced veins with a fewer number of mesophyll cells between two
572 consecutive veins (Fig. 5B). Those wild species also had larger mesophyll cell size, and thus a
573 lesser number of mesophyll cells per unit leaf area (Fig. 5C, D). We, then, quantified attributes

574 related to the mesophyll cell surface area of the selected accessions. Wild rice species, *O.*
575 *australiensis* and *O. latifolia*, showed remarkably higher average mesophyll cell surface area
576 as well as total mesophyll cell surface area per unit leaf area as compared to cultivated varieties
577 (Fig. 5E, F). We also investigated the organization of chloroplasts in mesophyll cells of the
578 representative wild and cultivated leaf. Photosynthetically efficient wild rice exhibited larger
579 and numerous chloroplasts, systematically distributed along the mesophyll cell walls
580 (Supplementary Fig. S6). These results underline the strong influence of mesophyll and
581 vascular features in determining leaf photosynthesis per unit area in rice.
582
583 **Discussion**
584 The importance of investigating variations in leaf photosynthesis within and across
585 species to be exploited for sustainable increases in crop yield and productivity has been
586 emphasized (Adachi *et al*. 2019; Ort *et al*., 2015; Simkin *et al*., 2019; van Bezouw *et al*., 2019).
587 A number of studies have shown the variation in photosynthesis and related traits within
588 species, such as wheat (Driever *et al*., 2014), rice (Giuliani *et al*., 2013; Qu *et al*., 2017), and
589 even C_4 species maize (Yabiku and Ueno, 2017), and *Gynandropsis gynandra* (Reeves *et al*.,
590 2018). Exploiting the photosynthetic variations within the rice system itself, including
591 cultivated and wild rice, is considered to be one of the potential strategies to increase genetic
592 yield potential. In this study, we not only quantified leaf photosynthetic differences across the
593 selected cultivated and wild rice accessions but also identified the biochemical limitations to
594 leaf photosynthesis per unit area in the selected cultivated varieties, IR64 and Nipponbare. In
595 addition, we also identified photochemical and leaf developmental traits associated with higher
596 leaf photosynthesis in selected wild rice species, *O. australiensis* and *O. latifolia*.
597 Wild relatives of rice, *O. australiensis*, *O. latifolia*, and *O. rufipogon*, as well as African
598 domesticated rice *O. glaberrima,* showed higher leaf photosynthesis per unit area (A) compared
599 to cultivated varieties of *Oryza sativa* (Fig. 1A). Stomatal conductance (g_s) and mesophyll
600 conductance (g_m) are known to be important factors determining the leaf photosynthesis rate
601 by regulating the leaf gaseous exchange (Gago *et al*., 2016; Kusumi *et al*., 2012; Xu *et al*.,
602 2019). Two wild rice species, *O. australiensis* and *O. latifolia*, with highest A, also had the
603 highest values of g_s and g_m, facilitating higher CO_2 concentration in intercellular spaces (C_i) as
604 well as inside mesophyll cells of those species (Fig. 1B, C; Table 1). *O. rufipogon* with
605 reasonably higher A, however, had lower g_s and Ci. The higher A in *O. rufipogon* was likely
606 due to high carboxylation efficiency (CE) in the species (Fig. 1D). Further, *O. australiensis*
607 and *O. latifolia* also had reasonably higher CE. The A has been shown to be positively

608 associated with *CE* in rice (Yeo *et al*., 1994). Indeed, quantification of photosynthesis and
609 related physiological parameters for introgressions from *O. rufipogon* in a cultivated
610 background showed the influence of both *CE* as well as g_s on higher leaf photosynthesis
611 (Haritha *et al*., 2017). Furthermore, higher g_s could also explain higher *A* across different PPFD
612 in the selected wild rice (Fig. 2A, B). The differences in g_s are likely related to differences in
613 the stomatal features or regulation of stomatal opening across the genotypes, as stomatal
614 features are critical for photosynthesis and gas exchange (Farquhar and Sharkey, 1982).
615 Comparison of several cultivated and wild rice genotypes had shown a close positive relation
616 between *A* and g_m, and g_m could increase leaf photosynthesis per unit area without affecting
617 transpiration (Flexas *et al*., 2008; Zhu *et al*., 2010; Giuliani *et al*., 2013). Differences in internal
618 CO_2 concentration and/or biochemical differences, such as Rubisco activity, may mediate the
619 observed differences in the *CE* (Eichelmann and Laisk, 2002). Nonetheless, efforts to increase
620 g_s, g_m, and *CE* in the cultivated rice varieties comparable to the high photosynthetic wild
621 species will help in increasing photosynthetic efficiency.

622 Fitting A/C_i curves along with quantification of photochemical features and Rubisco
623 activity assay showed that Rubisco carboxylation rate (V_{cmax}), and electron transport rate (J_{max})
624 were limiting to leaf photosynthesis per unit area in cultivated rice varieties IR 64 and
625 Nipponbare. Rubisco is the rate-limiting enzyme for photoassimilation of CO_2, and Rubisco
626 abundance and activity strongly determine the photosynthetic performance of a plant (Parry *et*
627 *al*., 2013; Sage, 2002). High photosynthetic wild species had higher expression of genes
628 encoding Rubisco large subunit and small subunit, indicating the higher abundance of Rubisco
629 in those species (Fig. 4C). Higher Rubisco activity per unit leaf area in the selected wild species
630 compared to the cultivated varieties could be due to either more Rubisco per unit area or the
631 presence of an efficient Rubisco in the wild species. Thick leaves of the photosynthetically
632 efficient wild species would support the first alternative where increasing leaf thickness would
633 lead to more Rubisco per unit area. More Rubisco per unit area, in addition, could also be
634 achieved by more nitrogen allocation to Rubisco. Furthermore, the possibility of the existence
635 of an efficient Rubisco in photosynthetically efficient wild rice species *O. latifolia* and *O.*
636 *australiensis* cannot be ruled out. The prospects of improving Rubisco catalysis to increase
637 photosynthetic efficiency have been explored (Sharwood, 2017). Cross-species Rubisco
638 engineering, for example maize Rubisco in rice, has been suggested to improve CO_2
639 assimilation (Parry *et al*., 2013; Sharwood *et al*., 2016b). Likewise, engineering wild rice
640 rubisco in the cultivated rice background could possibly overcome the Rubisco limitation of
641 photosynthesis in the cultivated varieties to some extent. Further studies will be needed to

642 investigate if there are differences in Rubisco kinetic properties across photosynthetically
643 contrasting cultivated and wild rice that might contribute to differences in Rubisco
644 carboxylation activity.

645 The comparative higher values for the quantum efficiency of PSII (*ϕPSII*) and
646 photochemical quenching (*qP*) along with J_{PSII} in *O. australiensis* and *O. latifolia* indicate more
647 receptive PSII reaction centers for electron transport from PSII to PSI in those species, making
648 an efficient link between light and light-independent reactions to increase *A* (Fig. 3A-C)
649 (Kramer and Evans, 2011). These desirable photochemical features, at least in part, contribute
650 to higher photosynthetic efficiency of the selected wild species. Gene expression studies also
651 showed higher expression of the *LHC1* gene, which is involved in the organization of reaction
652 center, in photosynthetically efficient wild species. Results, further, showed higher expression
653 of chlorophyll biosynthetic genes and higher chlorophyll content in those wild species, aiding
654 to the efficient light harvesting (Fig. 1E, 4D). Understanding the differential regulation of genes
655 encoding components of photosystem as well as chlorophyll biosynthesis in the wild species
656 could possibly help in improving photochemical features in the cultivated varieties.

657 The strong correlation of leaf developmental traits with *A* is not surprising considering
658 the strong influence of leaf traits on light perception, gas exchange, CO_2 assimilation, and
659 downstream photoassimilate partitioning. We observed a strong positive association of *A* with
660 leaf width and thickness (Fig. 5A). Leaf thickness has been suggested to influence
661 photosynthesis through efficient absorption and utilization of the light by homogenizing the
662 leaf internal light distribution as well as maintaining leaf temperature (Tholen *et al*., 2012).
663 Increasing leaf thickness, and thus more tissue per unit area would be instrumental for more
664 Rubisco, chlorophyll, and electron transport machinery per unit area. Higher chlorophyll and
665 electron transport machinery per unit area would facilitate efficient light harvesting for RuBP
666 regeneration, whereas more Rubisco content per unit leaf area would increase carboxylation
667 efficiency. Thus, targeting leaf thickness, similar to the photosynthetically efficient wild rice,
668 may result in high net photosynthesis per unit leaf area in the cultivated varieties by overcoming
669 Rubisco and electron transport rate limitations. Such leaves would indeed be beneficial under
670 high light intensity, but may not be optimal for light harvesting and photosynthesis under low
671 light conditions. Nonetheless, increasing leaf thickness could possibly be a potential way to
672 overcome the biochemical limitation of photosynthesis in the cultivated rice varieties under
673 ambient light conditions. The association of leaf width with photosynthetic performance and
674 yield in rice has been observed earlier. *WUSCHEL-RELATED HOMEOBOX* (*WOX*) genes
675 *NAL1*, *NAL2*, and *NAL3* have been shown to be associated with increased leaf width, which in

676 turn results in increased photosynthetic efficiency and yield (Fujita *et al*., 2013; Ishiwata *et al*.,
677 2013). Introgression of a natural variant of *NAL1* from *japonica* to *indica* cultivar led to thicker
678 and wider leaves with higher leaf photosynthesis rate and yield (Takai *et al*., 2013).

679 The rice system also displays significant inter-species variation for anatomical traits,
680 suggesting strong genetic control over leaf anatomical features (Chatterjee *et al*., 2016).
681 Photosynthetically efficient wild rice species have mesophyll cell features that promote both
682 higher accesses to available CO_2 as well as efficient light harvesting. Larger sized and lobed
683 mesophyll cells in wild rice species likely provide increased surface area to access more
684 internal CO_2 (Fig. 5B, C), whereas the organized pattern and systematic distribution of
685 chloroplasts in the mesophyll cells of those species may promote efficient light capture to
686 enhance photosynthesis (Fig. S6). Interestingly, *NAL1* (discussed above) promotes leaf width
687 and thickness by increasing mesophyll cell number and area. Lesser number of mesophyll cells
688 between two consecutive veins in photosynthetically efficient wild species, a feature similar to
689 C_4 plants, would be promoting efficient transport of photoassimilate (Amiard *et al*., 2005;
690 Feldman *et al*., 2017). Larger vein size in the wild rice species would, further, be adding to
691 efficient transport, thus increasing the leaf photosynthesis. Thus, photosynthetically efficient
692 wild rice species with desirable anatomical features provide a potential genetic resource
693 towards the identification of genes for desirable manipulation in mesophyll and vein features.

694 In summary, we identified biochemical limitations to leaf photosynthesis per unit area
695 in the selected cultivated rice varieties, IR64 and Nipponbare, compared to photosynthetically
696 efficient wild rice, *O. australiensis* and *O. latifolia*. Rubisco carboxylation activity and electron
697 transport rate along with photochemical features (quantum efficiency of PSII and
698 Photochemical quenching) and leaf developmental features (thicker and wider leaves, larger
699 and lobbed mesophyll cells, larger veins, and lesser number of mesophyll cells between two
700 consecutive veins) contribute to higher leaf photosynthesis in *O. australiensis* and *O. latifolia*
701 (Fig. 6). The study highlights the existence of significant exploitable variation in leaf
702 photosynthesis and underlying traits across cultivated and wild rice. Future efforts to dissect
703 the genetic and molecular basis of the underlying biochemical, photochemical, and
704 developmental traits shall be instrumental in tailoring photosynthetically efficient rice towards
705 the possible increases in genetic yield potential.
706
707
708
709

710 **Supplementary data**

711 **Fig. S1** Pair-wise correlation coefficient (*r*) analysis among the leaf photosynthesis and
712 physiological traits.

713

714 **Fig. S2.** Representative images of growth-chambers-grown plants of the selected cultivated
715 and wild rice accessions.

716

717 **Fig. S3.** Linear regression analysis between V_{cmax} and J_{max}, *TPU* and J_{max}, and V_{cmax} and *TPU*.

718

719 **Fig. S4.** Response and correlation of leaf photosynthesis (*A*) and electron transport rate (J_{PSII})
720 at varying CO_2 concentrations for the selected rice accessions.

721

722 **Fig. S5.** Flag leaf width and thickness of the selected cultivated and wild rice accessions.

723

724 **Fig. S6** TEM images for the organization of chloroplasts in mesophyll cells.

725

726 **Table S1.** Details of rice accessions used in the present study.

727

728 **Table S2.** Total chlorophyll content (*TCC*, μmol m^{-2}) and leaf absorbance (α) of fully-grown
729 eighth leaves of plants grown under controlled conditions.

730

731 **Table S3.** Details of genes used for expression analysis.

732

733 **Table S4.** List of primers for qRT-PCR analysis.

734

735 **Table S5.** Quantification of leaf photosynthesis and related physiological traits of fully-grown
736 eighth leaves of plants grown under controlled conditions.

737

738 **Table S6.** A_c-A_j and A_j-A_t transitions for the selected genotypes.

739

740 **Table S7.** Quantification of leaf developmental traits of the fully expanded flag leaves of the
741 selected cultivated rice varieties and wild rice species.

742

743

Acknowledgments

This work was supported by the core funding from the National Institute of Plant Genome Research as well as Ramalingaswamy Re-entry Fellowship (BT/RLF/Re-entry/05/2013) and Innovative Young Biotechnologist Award (BT/09/IYBA/2015/01) from the Department of Biotechnology, Ministry of Science and Technology, India. JM, AS, and VJ acknowledge their CSIR-JRF, SERB-NPDF, and UGC-JRF, fellowships, respectively. Seeds of wild rice species and *Oryza glaberrima* were kindly provided by Dr. Kuldeep Singh and Dr. Kumari Neelam, Punjab Agricultural University, Ludhiana, India.

Author contributions

JM and AR conceptualized the study. JM, AS, VJ, and AR designed experiments. JM, AS, and VJ performed experiments, analyzed data, and compiled figures. AS and AR wrote the manuscript. All authors contributed to and edited the final manuscript.

Data availability statement

Data sharing is not applicable to this article as all created data is already contained within this article or in the supplementary material.

References

Acevedo-Siaca LG, Coe R, Wang Y, Kromdijk W, Quick WP, Long SP. 2020. Variation in photosynthetic induction between rice accessions and its potential for improving productivity. New Phytologist **227**, 1097-1108.

Adachi S, Yamamoto T, Nakae T, Yamashita M, Uchida M, Karimata R Ichihara N, Soda K, Ochiai T, Ao R, Otsuka C, Nakano R, Takai T, Ikka T, Kondo K, Ueda T, Ookawa T, Hirasawa T. 2019. Genetic architecture of leaf photosynthesis in rice revealed by different types of reciprocal mapping populations. Journal of Experimental Botany **70**, 5131–5144.

Alexandratos N, Bruinsma J. 2012. World agriculture towards 2030/2050: the 2012 revision Global Perspective Studies Team FAO Agricultural Development Economics Division. Agricultural Development Economics (ESA) The Food and Agriculture Organization of the United Nations Viale delle Terme di Caracalla 00153 Rome, Italy.

Amiard V, Mueh KE, Demmig-Adams B, Ebbert V, Turgeon R, Adams WW. 2005. Anatomical and photosynthetic acclimation to the light environment in species with differing mechanisms of phloem loading. Proceedings of the National Academy of Sciences of the USA **102**, 12968–12973.

Arnon DI. 1949. Copper enzymes in isolated chloroplasts, polyphenol oxidase in Beta vulgaris. Plant Physiology **2**, 1-15.

Bernacchi CJ, Singsaas EL, Pimentel C, Portis Jr AR, Long SP. 2001. Improved temperature response functions for models of Rubisco-limited photosynthesis. Plant, Cell and Environment **24**, 253–259.

van Bezouw RFHM, Keurentjes JJB, Harbinson J, Aarts MGM. 2019. Converging phenomics and genomics to study natural variation in plant photosynthetic efficiency. Plant Journal **97**, 112–133.

Brodribb TJ, Feild TS, Jordan GJ. 2007. Leaf maximum photosynthetic rate and venation are linked by hydraulics. Plant Physiology **144**, 1890–1898.

Busch FA. 2018. Photosynthetic gas exchange in land plants at the leaf level. In Covshoff S ed., Photosynthesis: Methods and Protocols, Methods in Molecular Biology, vol. 1770, 25 - 44.

von Caemmerer S. 2000. Biochemical Models of Leaf Photosynthesis, pp. 1–165. CSIRO Publishing, Collingwood, Victoria, Australia.

Cardona T, Shao S, Nixon PJ. 2018. Enhancing photosynthesis in plants: the light reactions.

Essays In Biochemistry **62**, 85–94.

Chatterjee J, Dionora J, Elmido-Mabilangan A, Wanchana S, Thakur V, Bandyopadhyay A, Brar DS, Quick WP. 2016. The evolutionary basis of naturally diverse rice leaves anatomy. PLoS ONE **11**, 1–25.

De Souza AP, Wang Y, Orr DJ, Carmo-Silva E, Long SP. 2020. Photosynthesis across African cassava germplasm is limited by Rubisco and mesophyll conductance at steady state, but by stomatal conductance in fluctuating light. New Phytologist **225**, 2498– 2513.

Driever SM, Lawson T, Andralojc PJ, Raines CA, Parry MAJ. 2014. Natural variation in photosynthetic capacity, growth, and yield in 64 field-grown wheat genotypes. Journal of Experimental Botany **65**, 4959–4973.

Eichelmann H, Laisk A. 2002. Ribulose-1,5-bisphosphate carboxylase/oxygenase content, assimilatory charge, and mesophyll conductance in leaves. Plant Physiology **119**, 179–190.

Evans JR, Poorter H. 2001. Photosynthetic acclimation of plants to growth irradiance: the relative importance of SLA and nitrogen partitioning in maximising carbon gain. Plant, Cell and Environment **24**, 755–768.

Evans JR. 2013. Improving photosynthesis. Plant Physiology **162**, 1780–1793.

Fabre D, Yin X, Dingkuhn M, Clément-Vidal A, Roques S, Rouan L, Soutiras A, Delphine L. 2019. Is triose phosphate utilization involved in the feedback inhibition of photosynthesis in rice under conditions of sink limitation? Journal of Experimental Botany **70**, 5773–5785.

Farquhar GD, von Caemmerer S, Berry JA. 1980. A biochemical model of photosynthetic CO_2 assimilation in leaves of C_3 species. Planta **149**, 78–90.

Farquhar GD, Sharkey TD. 1982. Stomatal conductance and photosynthesis. Annual Review of Plant Physiology **33**, 317–345.

Feldman AB, Leung H, Baraoidan M, Elmido-mabilangan A. 2017. Increasing leaf vein density via mutagenesis in rice results in an enhanced rate of photosynthesis, smaller cell sizes and can reduce interveinal mesophyll cell number. Frontiers in Plant Science **8**, 1–10.

Flexas J, Ribas-Carbó M, Diaz-Espejo A, Galmés J, Medrano H. 2008. Mesophyll conductance to CO_2: Current knowledge and future prospects. Plant, Cell and Environment **31**, 602–621.

Flood PJ, Harbinson J, Aarts MGM. 2011. Natural genetic variation in plant photosynthesis.

Trends in Plant Science 16, 327-335.

Fujita D, Trijatmiko KR, Tagle AG, Sapasap MV, Koide Y, Sasaki K, *et al.* 2013. NAL1 allele from a rice landrace greatly increases yield in modern indica cultivars. Proceedings of the National Academy of Sciences of the USA **110**, 20431–20436.

Gago J, Daloso DdeM, Figueroa CM, Flexas J, Fernie AR, Nikoloski Z. 2016. Relationships of leaf net photosynthesis, stomatal conductance, and mesophyll conductance to primary metabolism: A multispecies meta-analysis approach. Plant Physiology **171**, 265–279.

Giuliani R, Koteyeva N, Voznesenskaya E, Evans MA, Cousins AB, Edwards GE. 2013. Coordination of leaf photosynthesis, transpiration, and structural traits in rice and wild relatives (Genus Oryza). Plant Physiology **162**, 1632–1651.

Haritha G, Vishnukiran T, Yugandhar P, Sarla N, Subrahmanyam D. 2017. Introgressions from *Oryza rufipogon* increase photosynthetic efficiency of KMR3 Rice Lines. Rice Science **24**, 85–96.

Harley PC, Loreto F, Marco GDi, Sharkey TD. 1992. Theoretical considerations when estimating the mesophyll conductance to CO_2 flux by analysis of the response of photosynthesis to CO_2. Plant Physiology **98**, 1429–1436.

Hiyama A, Takemiya A, Munemasa S, Okuma E, Sugiyama N, Tada Y, Murata Y, Shimazaki KI. 2017. Blue light and CO_2 signals converge to regulate light-induced stomatal opening. Nature Communications **8,** 1284.

Ishiwata A, Ozawa M, Nagasaki H, Kato M, Noda Y, Yamaguchi T, Nosaka M, Shimizu-Sato S, Nagasaki A, Maekawa M, Hirano H-Y, Sato Y. 2013. Two WUSCHEL-related homeobox genes, narrow leaf2 and narrow leaf3, control leaf width in rice. Plant and Cell Physiology **54**, 779–792.

Ivanova LA, Yudina PK, Ronzhina DA, Ivanov LA, Hölzel N. 2018. Quantitative mesophyll parameters rather than whole-leaf traits predict response of C_3 steppe plants to aridity. New Phytologist **217**, 558–570.

Kajala K, Covshoff S, Karki S, Woodfield H, Tolley BJ, Dionora MJA, Mogul RT, Mabilangan AE, Danila FR, Hibberd JM, Quick WP. 2011 Strategies for engineering a two-celled C_4 photosynthetic pathway into rice. Journal of Experimental Botany **62**, 3001–3010.

Kalaji HM, Jajoo A, Oukarroum A, Brestic M, Zivcak M, Samborska IA, Cetner MD, Lukasik I, Goltsev V, Ladle RJ. 2016 Chlorophyll a fluorescence as a tool to monitor physiological status of plants under abiotic stress conditions. Acta Physiologiae Plantarum

38, 102.

Kimball BA. 2016. Crop responses to elevated CO_2 and interactions with H_2O, N, and temperature. Current Opinion in Plant Biology **31**, 36–43.

Koteyeva NK, Voznesenskaya EV, Berry JO, Chuong SDX, Franceschi VR, Edwards GE. 2011. Development of structural and biochemical characteristics of C_4 photosynthesis in two types of Kranz anatomy in genus Suaeda (family Chenopodiaceae). Journal of Experimental Botany **62**, 3197–3212.

Kramer DM, Evans JR. 2011. The Importance of energy balance in improving photosynthetic productivity. Plant Physiology **155**, 70–78.

Kromdijk J, Głowacka K, Leonelli L, Gabilly ST, Iwai M, Niyogi KK, Long SP. 2016. Improving photosynthesis and crop productivity by accelerating recovery from photoprotection. Science **354**, 857–861.

Kubien DS, Brown CM, Kane HJ. 2011. Quantifying the amount and activity of rubisco in leaves. Photosynthesis Research Protocol **684**, 349–362.

Kumarathunge DP, Medlyn BE, Drake JE, Rogers A, Tjoelker MG. 2019. No evidence for triose phosphate limitation of light-saturated leaf photosynthesis under current atmospheric CO_2 concentration. Plant, Cell and Environment **42**, 3241-3252.

Kusumi K, Hirotsuka S, Kumamaru T, Iba K. 2012. Increased leaf photosynthesis caused by elevated stomatal conductance in a rice mutant deficient in SLAC1, a guard cell anion channel protein. Journal of Experimental Botany **63,** 5635– 5644.

Laisk AK. 1977. Kinetics of photosynthesis and photorespiration in C_3-Plants. Nauka, Moscow

Lawson T, Kramer DM, Raines CA. 2012. Improving yield by exploiting mechanisms underlying natural variation of photosynthesis. Current Opinion in Biotechnology **23**, 215–220.

Li Y, Gao Y, Xu X, Shen Q, Guo S. 2009. Light-saturated photosynthetic rate in high-nitrogen rice (*Oryza sativa* L.) leaves is related to chloroplastic CO_2 concentration. Journal of Experimental Botany **60,** 2351–2360.

Lin MT, Occhialini A, Andralojc PJ, Parry MAJ & Hanson MR. 2014. A faster Rubisco with potential to increase photosynthesis in crops. Nature **513**, 547–550

Liu L, Sun G, Ren X, Li C, Sun D. 2015. Identification of QTL underlying physiological and morphological traits of flag leaf in barley. BMC Genetics **16**, 29.

Livak KJ, Schmittgen TD. 2001. Analysis of relative gene expression data using real-time quantitative PCR and the $2^{-\Delta\Delta CT}$ method. Methods **25**, 402–408.

Long SP, Bernacchi CJ. 2003. Gas exchange measurements, what can they tell us about the underlying limitations to photosynthesis? Procedures and sources of error. Journal of Experimental Botany **54**, 2393–2401.

Long SP, Zhu XG, Naidu SL, Ort DR. 2006. Can improvement in photosynthesis increase crop yields? Plant, Cell and Environment **29**, 315–330.

Lux A, Morita S, Abe J, Ito K. 2005. An improved method for clearing and staining free-hand sections and whole-mount samples. Annals of Botany **96**, 989–996.

Mathan J, Bhattacharya J, Ranjan A. 2016. Enhancing crop yield by optimizing plant developmental features. Development **143**, 3283–3294.

Murchie EH, Lawson T. 2013. Chlorophyll fluorescence analysis: A guide to good practice and understanding some new applications. Journal of Experimental Botany **64**, 3983–3998.

Murchie EH, Niyogi KK. 2011. Manipulation of photoprotection to improve plant photosynthesis. Plant Physiology **155**, 86–92.

Ort DR, Merchant SS, Alric J, Barkan A, Blankenship RE, *et al.* 2015. Redesigning photosynthesis to sustainably meet global food and bioenergy demand. Proceedings of the National Academy of Sciences of the USA **112,** 8529-8536.

Parry MAJ, Madgwick PJ, Carvahlo JFC, Andralojc PJ. 2007. Prospects for increasing photosynthesis by overcoming the limitations of Rubisco. Journal of Agricultural Science **145**, 31-43.

Parry MAJ, Andralojc PJ, Scales JC, Salvucci ME, Carmo-Silva AE, Alonso H, Whitney SM. 2013. Rubisco activity and regulation as targets for crop improvement. Journal of Experimental Botany **64**, 717-730.

Peng S, Khush GS, Virk P, Tang Q, Zou Y. 2008. Progress in ideotype breeding to increase rice yield potential. Field Crops Research **108**, 32–38.

Perdomo JA, Capó-Bauçà S, Carmo-Silva E and Galmés J. 2017. Rubisco and rubisco activase play an important role in the biochemical limitations of photosynthesis in rice, wheat, and maize under high temperature and water deficit. Frontiers in plant science **8**, 1-15.

Porra RJ, Thompson WA, Kriedemann PE. 1989. Determination of accurate extinction coefficients and simultaneous equations for assaying chlorophylls a and b extracted with four different solvents: Verification of the concentration of chlorophyll standards by atomic absorption spectroscopy. Biochim Biophys Acta Bioenerg **975**, 384–394.

Qu M, Zheng G, Hamdani S, Essemine J, Song Q, Wang H, Chu C, Sirault X, Zhu XG.

2017. Leaf photosynthetic parameters related to biomass accumulation in a global rice diversity survey. Plant Physiology **175**, 248–258.

Reeves G, Singh P, Rossberg TA, Sogbohossou EOD, Schranz ME, Hibberd JM. 2018. Natural variation within a species for traits underpinning C_4 photosynthesis. Plant Physiology **177**, 504–512.

Reynolds ES. 1963. The use of lead citrate at high pH as an electron-opaque stain in electron microscopy. The Journal of Cell Biology **17**, 208–212.

Rogers A, Allen DJ, Davey PA, Morgan PB, Ainsworth EA, Bernacchi CJ, Cornic G, Dermody O, Dohleman FG, Heaton EA, Mahoney J, Zhu XG, Delucia EH, Ort DR, Long SP. 2004. Leaf photosynthesis and carbohydrate dynamics of soybeans grown throughout their life-cycle under Free-Air Carbon dioxide Enrichment. Plant, Cell and Environment **27**, 449–458.

Rosenthal DM, Slattery RA, Miller RE, Grennan AK, Cavagnaro TR, Fauquet CM, Gleadow RM, Ort DR. 2012. Cassava about-FACE: Greater than expected yield stimulation of cassava (Manihot esculenta) by future CO_2 levels. Global Change Biology **18**, 2661–2675.

Sage RF. 2002. Variation in the kcat of Rubisco in C_3 and C_4 plants and some implications for photosynthetic performance at high and low temperature. Journal of Experimental Botany **53**, 609–620.

Sage TL, Sage RF. 2009 The functional anatomy of rice leaves: Implications for refixation of photorespiratory CO_2 and efforts to engineer C_4 photosynthesis into rice. Plant and Cell Physiology **50**, 756–772.

Sanchez PL, Wing RA, Brar DS. 2013. The wild relative of Rice: Genomes and Genomics. Genetics and Genomics of Rice **5**, 9-25.

Sharkey TD. 1984. Photosynthesis in intact leaves of C_3 plants: Physics, physiology and rate limitations. Botanical Review 51, 53-105.

Sharkey TD, Bernacchi CJ, Farquhar GD, Singsaas EL. 2007. Fitting photosynthetic carbon dioxide response curves for C_3 leaves. Plant, Cell and Environment **30**, 1035–1040.

Sharkey TD. 2016. What gas exchange data can tell us about photosynthesis. Plant, Cell and Environment **39**, 1161–1163.

Sharwood RE, Sonawane BV, Ghannoum O, Whitney SP. 2016a. Improved analysis of C_4 and C_3 photosynthesis via refined *in vitro* assays of their carbon fixation biochemistry. Journal of Experimental Botany, **67**, 3137–3148.

Sharwood RE, Ghannoum O, Whitney SM. 2016b. Prospects for improving CO_2 fixation in C_3-crops through understanding C_4-Rubisco biogenesis and catalytic diversity. Current Opinion in Plant Biology **31**, 135–142.

Sharwood RE. 2017. Engineering chloroplasts to improve Rubisco catalysis: prospects for translating improvements into food and fiber crops. New Phytologist **213**, 494–510.

Simkin AJ, López-calcagno PE, Raines CA. 2019. Feeding the world : improving photosynthetic efficiency for sustainable crop production. Journal of Experimental Botany **70**, 1119–1140.

South PF, Cavanagh AP, Liu HW, Ort DR. 2019. Synthetic glycolate metabolism pathways stimulate crop growth and productivity in the field. Science **363**, 0-10.

Stein JC, Yu Y, Copetti D, Zwickl DJ, Zhang L, Zhang C *et al.* 2018. Genomes of 13 domesticated and wild rice relatives highlight genetic conservation, turnover and innovation across the genus Oryza. Nature Genetics **50**, 285–296.

Takai T, Adachi S, Taguchi-Shiobara F, Sanoh-Arai Y, Iwasawa N, Yoshinaga S, Hirose S, Taniguchi Y, Yamanouchi U, Wu J, Matsumoto T, Sugimoto K, Kondo K, Ikka T, Ando T, Kono I, Ito S, Shomura A, Ookawa T, Hirasawa T, Yano M, Kondo M, Yamamoto T. 2013. A natural variant of NAL1, selected in high-yield rice breeding programs, pleiotropically increases photosynthesis rate. Scientific Reports **3**, 1–11.

Tholen D, Boom C, Zhu XG. 2012. Opinion: prospects for improving photosynthesis by altering leaf anatomy. Plant Science **197**, 92–101.**Wu A, Hammer GL, Doherty A, von Caemmerer S, Farquhar GD.** 2019. Quantifying impacts of enhancing photosynthesis on crop yield. Nature plants **5**, 380-388.

Xu F, Wang K, Yuan W, Xu W, Shuang L, Kronzucker HJ, Chen G, Miao R, Zhang M, Ding M, Xiao L, Kai L, Zhang J, Zhu Y. 2019. Overexpression of rice aquaporin OsPIP1;2 improves yield by enhancing mesophyll CO_2 conductance and phloem sucrose transport. Journal of Experimental Botany **70**, 671–681.

Yabiku T, Ueno O. 2017. Variations in physiological, biochemical, and structural traits of photosynthesis and resource use efficiency in maize and teosintes (NADP-ME-type C_4). Plant Production Science **20**, 448–458.

Yeo ME, Yeo AR, Flowers TJ. 1994. Photosynthesis and photorespiration in the genus Oryza. Journal of Experimental Botany **45**, 553–560.

Zhu XG, Long SP, Ort DR. 2010. Improving photosynthetic efficiency for greater yield. Annual Review of Plant Biology **61**, 235–61.

Table 1. Mitochondrial respiration rate in the light (R_d), CO_2 compensation point related to C_i (Γ^*), and mesophyll conductance (g_m) for the selected cultivated and wild rice genotypes. Each value represents mean ± SE, where n = five data points from different plants. Different letters indicate statistically significant differences according to one-way ANOVA followed by post-hoc Tukey HSD calculation at $P \leq 0.05$.

Genotypes	R_d (µmol CO_2 m^{-2} s^{-1})	Γ^* (µmol CO_2 mol^{-1})	g_m (mol CO_2 m^{-2} s^{-1})
O. sativa cv. Nipponbare	1.05 ± 0.15a	43.8 ± 1.7a	0.12 ± 0.00a
O. sativa cv. IR 64	1.03 ± 0.10a	42.3 ± 3.0a	0.11 ± 0.01a
O. glaberrima	1.15 ± 0.16a	44.5 ± 2.0a	0.26 ± 0.03b
O. latifolia	1.37 ± 0.19b	45.4 ± 0.7a	0.33 ± 0.02c
O. australiensis	1.39 ± 0.18b	45.5 ± 0.8a	0.30 ± 0.05c

Table 2. Maximum photosynthesis (A_{max}), maximum *in vivo* Rubisco activity (V_{cmax}), maximum electron transport rate (J_{max}), and maximum rate of triose phosphate utilization (*TPU*) through A/C_i curve analysis. Each value represents mean ± SE, where n = five data points from different plants. Different letters indicate statistically significant differences according to one-way ANOVA followed by post-hoc Tukey HSD calculation at $P \leq 0.05$.

Genotypes	A_{max} (µmol m^{-2} s^{-1})	V_{cmax} (µmol m^{-2} s^{-1})	J_{max} (µmol m^{-2} s^{-1})	*TPU* (µmol m^{-2} s^{-1})
O. sativa cv. Nipponbare	22.29 ± 0.40b	62.75 ± 0.92b	124.86 ± 1.37b	8.48 ± 0.06b
O. sativa cv. IR 64	20.07 ± 0.88a	51.48 ± 2.69a	103.06 ± 3.19a	6.79 ± 0.19a
O. glaberrima	30.41 ± 0.14c	70.04 ± 0.79cd	149.21 ± 1.80c	10.28 ± 0.10c
O. latifolia	34.32 ± 0.39d	76.75 ± 1.24de	166.17 ± 2.86d	11.72 ± 0.27d
O. australiensis	36.81 ± 0.37e	81.25 ± 1.08e	181.93 ± 0.77e	12.27 ± 0.12d

Table 3. *in vitro* RuBP-use and Rubisco carboxylation rate (V_{cmax}) for selected rice genotypes. Each value represents mean ± SE, where n = five data points from different plants. The significant difference among the accession is indicated by different letters (one way ANOVA followed by Tukey's HSD, $P < 0.05$).

Genotypes	*RuBP-use* (nmol s^{-1})			V_{cmax} (µmol m^{-2} s^{-1})		
	120 s	180 s	240 s	120 s	180 s	240 s
O. sativa cv. Nipponbare	0.198 ± 0.01b	0.200 ± 0.01b	0.195 ± 0.01b	43.52 ± 1.50b	43.98 ± 1.43b	42.71 ± 1.40b
O. sativa cv. IR 64	0.166 ± 0.01a	0.168 ± 0.00a	0.165 ± 0.01a	36.37 ± 3.00a	36.91 ± 1.00a	36.22 ± 1.22a
O. glaberrima	0.231 ± 0.01cd	0.236 ± 0.00c	0.223 ± 0.00c	50.67 ± 1.71c	51.87 ± 0.87c	49.01 ± 0.85c
O. latifolia	0.256 ± 0.01d	0.261 ± 0.01d	0.245 ± 0.01cd	56.10 ± 1.30d	57.29 ± 1.35d	53.69 ± 1.39d
O. australiensis	0.282 ± 0.00d	0.284 ± 0.01d	0.260 ± 0.00d	61.99 ± 0.48d	62.22 ± 1.35d	57.02 ± 0.65d

Figure legends

Fig.1. Variations in leaf photosynthesis and related physiological features, as well as morphological differences across the selected cultivated and wild rice accessions.

(A-E) Quantification of net photosynthesis per unit area of flag leaf, *A* (A), stomatal conductance to water, g_s (B), intercellular CO_2 concentration, C_i (C), carboxylation efficiency, *CE* (D), and Total chlorophyll content, *TCC* (E) for six cultivated rice and three wild rice species. Cultivated rice varieties and wild species are represented with yellow- and green-shaded boxes, respectively. Each box plot shows the median and upper and lower quartiles of fifteen data points from different plants. Different letters indicate statistical significance according to one-way ANOVA followed by post-hoc Tukey HSD calculation at $P \leq 0.05$.

(F) Representative images of the selected cultivated and wild rice accessions that captured the entire variation range for the leaf photosynthesis per unit area in the experiment. Shown are the field-grown plants of the selected genotypes. Scale bars represent 30 cm.

Fig. 2. Effect of varying light intensity and CO_2 concentration on leaf photosynthesis and stomatal conductance.

(A-B) Quantification of net photosynthesis per unit leaf area, *A* (A) and stomatal conductance to water, g_s (B) in response to increasing PPFD from 100 to 2000 µmol m^2 s^{-1} at 400 µmol mol^{-1} CO_2 concentration.

(C-D) Quantification of net photosynthesis per unit leaf area, *A* (C) and stomatal conductance to water, g_s (D) in response to varying external CO_2 concentration (C_a) at 1500 µmol m^{-2} s^{-1} light intensity.

Each value represents mean ± SE, where n = five data points from different plants. Different letters at each light intensity and CO_2 concentration indicate statistical significance according to one-way ANOVA followed by post-hoc Tukey HSD calculation at $P \leq 0.05$.

Fig. 3. Photochemical features of the selected cultivated and wild rice accessions.

Quantification of electron transport rate, J_{PSII} (A), the efficiency of PSII, $\phi PSII$ (B), and photochemical quenching, *qP* (C) of the selected accessions at varying CO_2 concentrations. Each value represents mean ± SE, where n = five data points from different plants. Different letters at each CO_2 concentration indicate statistical significance according to one-way ANOVA followed by post-hoc Tukey HSD calculation at $P \leq 0.05$.

Fig. 4. RuBP-use, Rubisco activity, and gene expression differences across the selected accessions.

(A) NADH-linked spectrophotometric measurement of RuBP-use (nmol) at different time points from 10 to 1800 sec.

(B) Quantification of V_{cmax} for the selected accessions at different time points up to saturation.

(C) Expression levels of genes encoding a key component of the light-harvesting complex, Rubisco, and Triose phosphate/phosphate translocator.

(D) Expression levels of key chlorophyll biosynthetic genes.

Values represent mean ± SE. Different letters indicate statistical significance according to one-way ANOVA followed by post-hoc Tukey HSD calculation at $P \leq 0.05$.

Gene abbreviations: LHCI, Light-harvesting chlorophyll protein complex I; Rubisco SS, Ribulose bisphosphate carboxylase small subunit; Rubisco LS, Ribulose bisphosphate carboxylase large subunit; TPT, Triose phosphate/phosphate translocator; GluTR, Glutamyl-tRNA reductase; PPOX, Protoporphyrinogen oxidase; Mg-CHLD subunit ChlD, Magnesium chelatase; CHLSYN, Chlorophyll synthase; CAO, Chlorophyllide a oxygenase.

Fig. 5. Leaf developmental traits affecting photosynthesis rate and related physiological traits of rice.

(A) Correlation of leaf photosynthesis rate and related physiological traits with leaf developmental features. The red shade represents a significant positive correlation at $P \leq 0.05$.

(B) Bright-field images of a cross-section of a flag leaf of the selected genotypes showing variations in mesophyll cells and vasculature. Arrows indicate bulliform cells (bc), bundle sheath (bs), epidermis (ep), mesophyll cells (mc), and minor veins (miv). Scale bars represent 100 µm.

(C) Bright-field microscopy images showing variations in mesophyll cell features, including lobbing. Scale bar represents 10 µm.

(D-F) Quantification of total mesophyll cell number per unit leaf area (D), average mesophyll cell surface area (E), and total mesophyll cell surface area per unit leaf area (F) of selected cultivated and wild rice accessions. Cultivated rice accessions and wild species are represented with yellow- and green- shaded boxes, respectively. Each box plot shows the median and upper and lower quartiles. Different letters indicate statistical significance according to one-way ANOVA followed by post-hoc Tukey HSD calculation at $P \leq 0.05$.

Fig. 6. Leaf developmental, photochemical, and biochemical traits contributing towards photosynthetic differences between two extreme genotypes: *Oryza sativa* ssp. *indica* cv. IR 64 and *Oryza australiensis*. Wider leaf, larger mesophyll cells, larger veins, fewer number of mesophyll cells between two consecutive veins, more chloroplasts, efficient Electron Transport Rate along with higher Rubisco activity facilitate higher leaf photosynthesis per unit area in the wild rice species *Oryza australiensis* compared to the cultivated variety *Oryza sativa* ssp. *indica* cv. IR 64.

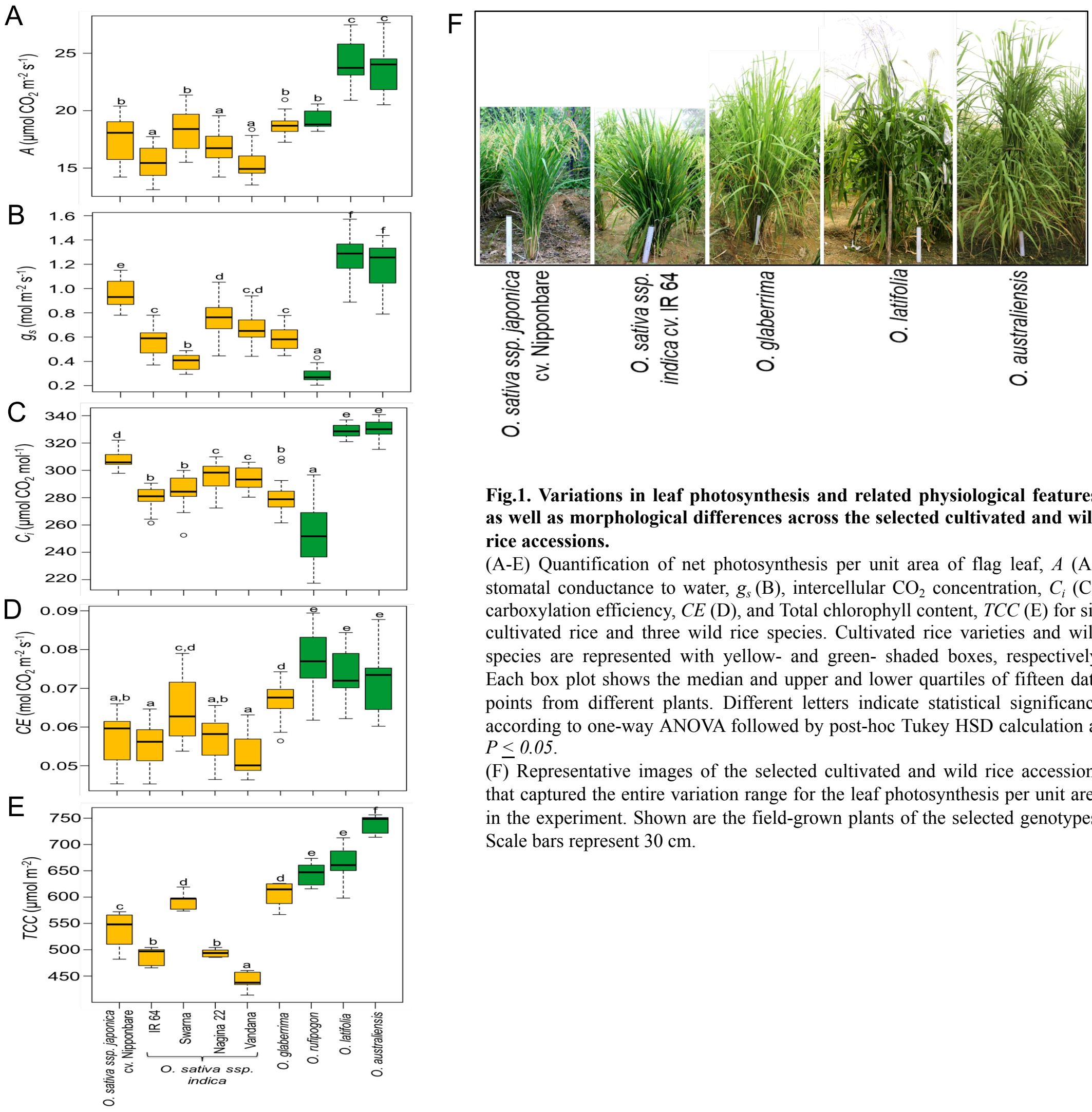

Fig.1. Variations in leaf photosynthesis and related physiological features, as well as morphological differences across the selected cultivated and wild rice accessions.

(A-E) Quantification of net photosynthesis per unit area of flag leaf, *A* (A), stomatal conductance to water, g_s (B), intercellular CO_2 concentration, C_i (C), carboxylation efficiency, *CE* (D), and Total chlorophyll content, *TCC* (E) for six cultivated rice and three wild rice species. Cultivated rice varieties and wild species are represented with yellow- and green- shaded boxes, respectively. Each box plot shows the median and upper and lower quartiles of fifteen data points from different plants. Different letters indicate statistical significance according to one-way ANOVA followed by post-hoc Tukey HSD calculation at $P \leq 0.05$.

(F) Representative images of the selected cultivated and wild rice accessions that captured the entire variation range for the leaf photosynthesis per unit area in the experiment. Shown are the field-grown plants of the selected genotypes. Scale bars represent 30 cm.

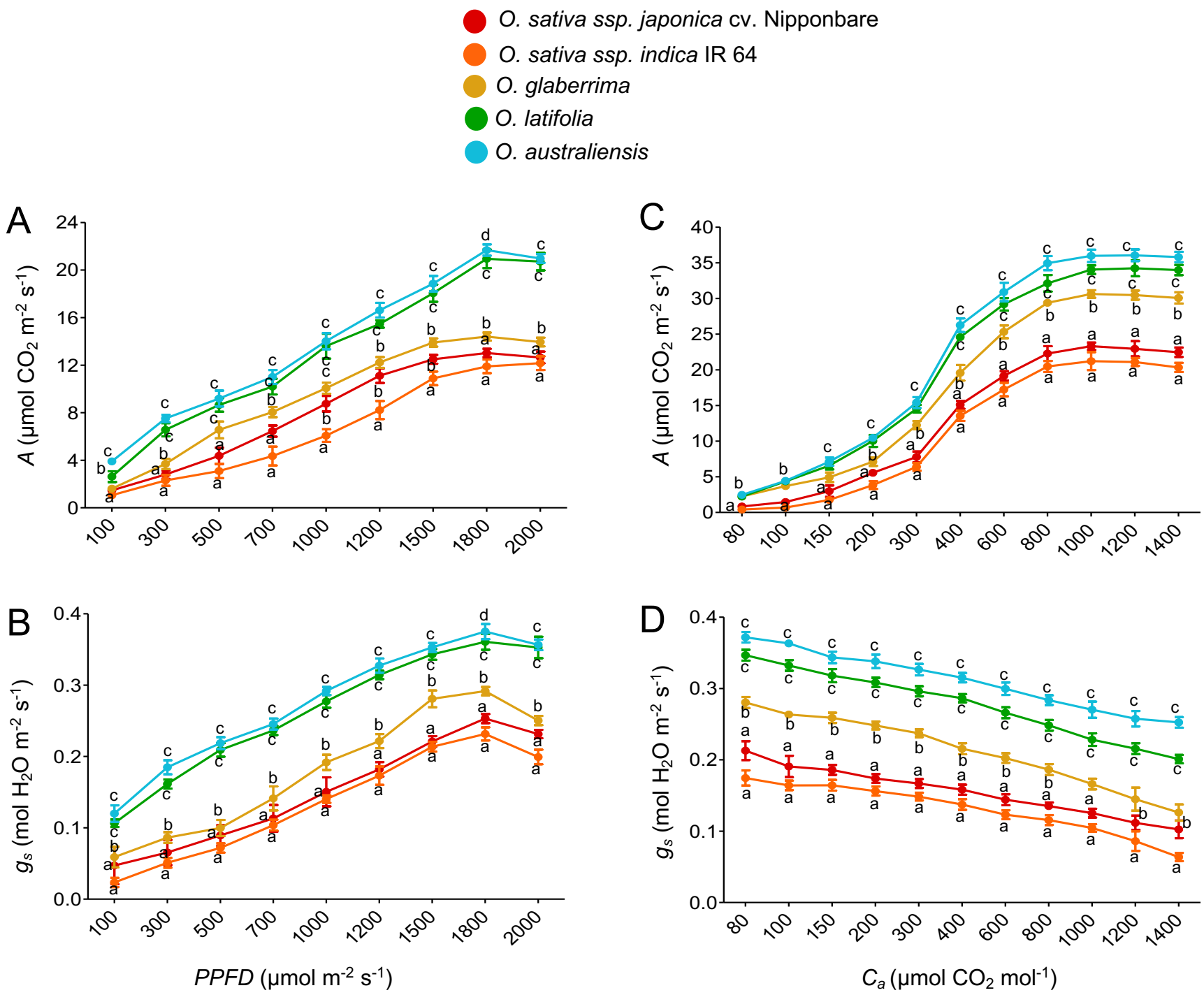

Fig. 2. Effect of varying light intensity and CO_2 concentration on leaf photosynthesis and stomatal conductance.
(A-B) Quantification of net photosynthesis per unit leaf area, *A* (A) and stomatal conductance to water, g_s (B) in response to increasing PPFD from 100 to 2000 µmol m^2 s^{-1} at 400 µmol mol^{-1} CO_2 concentration.
(C-D) Quantification of net photosynthesis per unit leaf area, *A* (C) and stomatal conductance to water, g_s (D) in response to varying external CO_2 concentration (C_a) at 1500 µmol m^{-2} s^{-1} light intensity.
Each value represents mean ± SE, where n = five data points from different plants. Different letters at each light intensity and CO_2 concentration indicate statistical significance according to one-way ANOVA followed by post-hoc Tukey HSD calculation at $P \leq 0.05$.

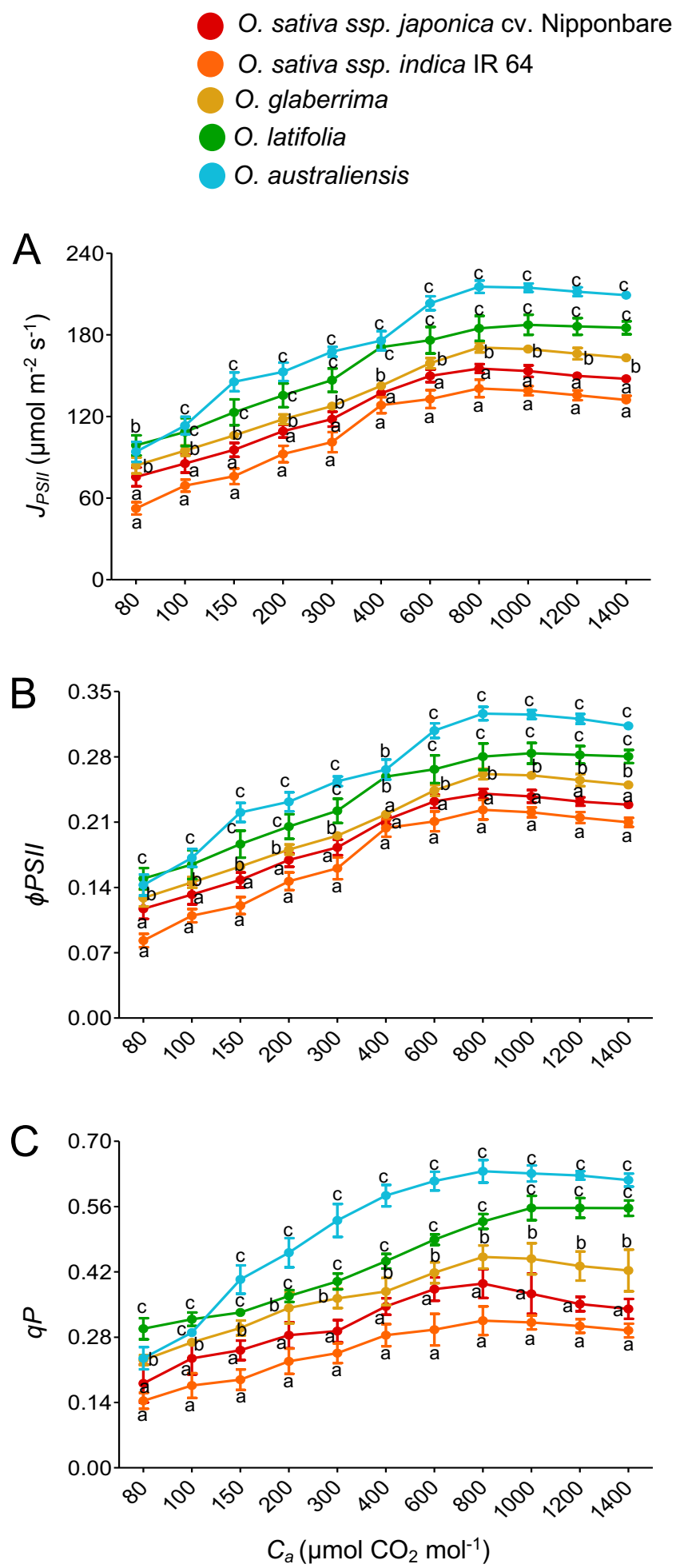

Fig. 3. Photochemical features of the selected cultivated and wild rice accessions.
Quantification of electron transport rate, J_{PSII} (A), the efficiency of PSII, *ϕPSII* (B), and photochemical quenching, *qP* (C) of the selected accessions at varying CO_2 concentrations. Each value represents mean ± SE, where n = five data points from different plants. Different letters at each CO_2 concentration indicate statistical significance according to one-way ANOVA followed by post-hoc Tukey HSD calculation at $P \leq 0.05$.

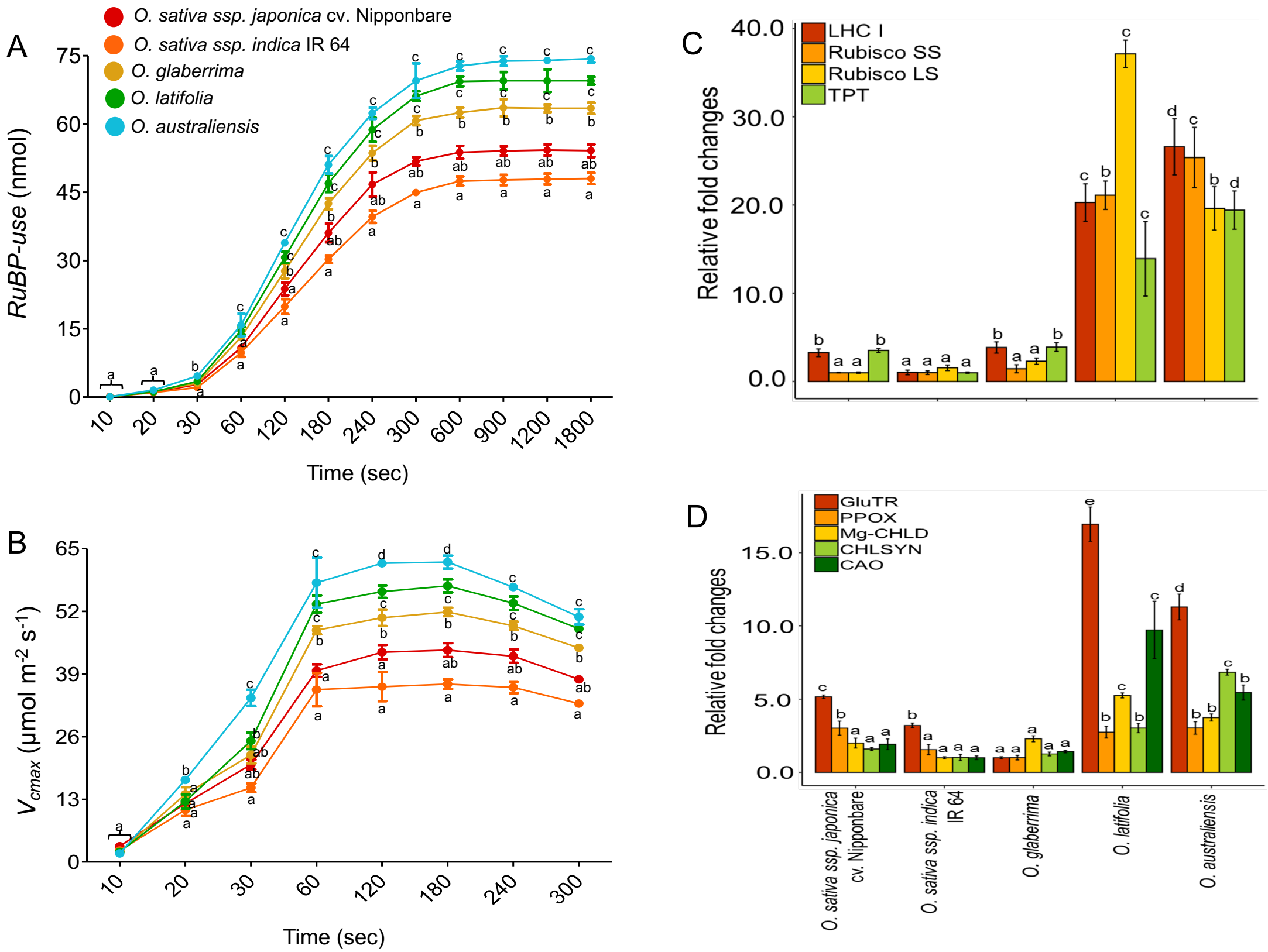

Fig. 4. RuBP-use, Rubisco activity, and gene expression differences across the selected accessions.
(A) NADH-linked spectrophotometric measurement of RuBP-use (nmol) at different time points from 10 to 1800 sec.
(B) Quantification of V_{cmax} for the selected accessions at different time points up to saturation.
(C) Expression levels of genes encoding a key component of the light-harvesting complex, Rubisco, and Triose phosphate/phosphate translocator.
(D) Expression levels of key chlorophyll biosynthetic genes.
Values represent mean ± SE. Different letters indicate statistical significance according to one-way ANOVA followed by post-hoc Tukey HSD calculation at $P \leq 0.05$.
Gene abbreviations: LHCI, Light-harvesting chlorophyll protein complex I; Rubisco SS, Ribulose bisphosphate carboxylase small subunit; Rubisco LS, Ribulose bisphosphate carboxylase large subunit; TPT, Triose phosphate/phosphate translocator; GluTR, Glutamyl-tRNA reductase; PPOX, Protoporphyrinogen oxidase; Mg-CHLD subunit ChlD, Magnesium chelatase; CHLSYN, Chlorophyll synthase; CAO, Chlorophyllide a oxygenase.

A

	Traits	A	g_s	C_i	CE
Morphological	*FLW*	0.850	0.469	0.369	0.758
	FLT	0.938	0.423	0.304	0.943
Vein	*MiV-W*	0.752	0.412	0.472	0.595
	MiV-H	0.899	0.596	0.597	0.708
	TV	0.848	0.415	0.326	0.786
Mesophyll	*M-Lo*	0.760	0.461	0.476	0.573
	M-L	0.863	0.557	0.442	0.734
	M-W	0.928	0.573	0.456	0.814
	M-A	0.924	0.580	0.454	0.814
Bundle sheath	*BS-No*	0.148	-0.397	-0.370	0.473
	BS-A	0.002	0.217	0.229	-0.164

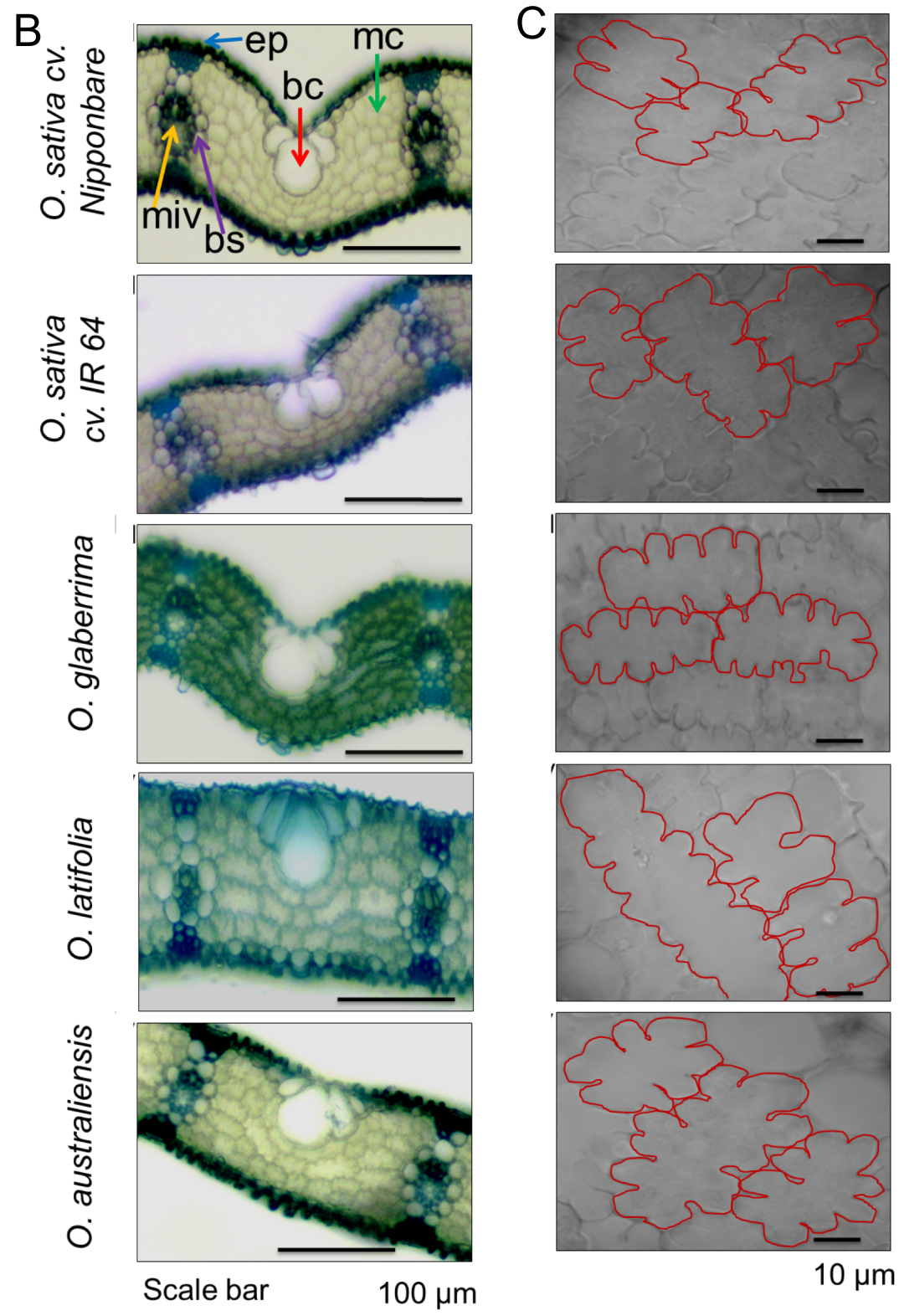

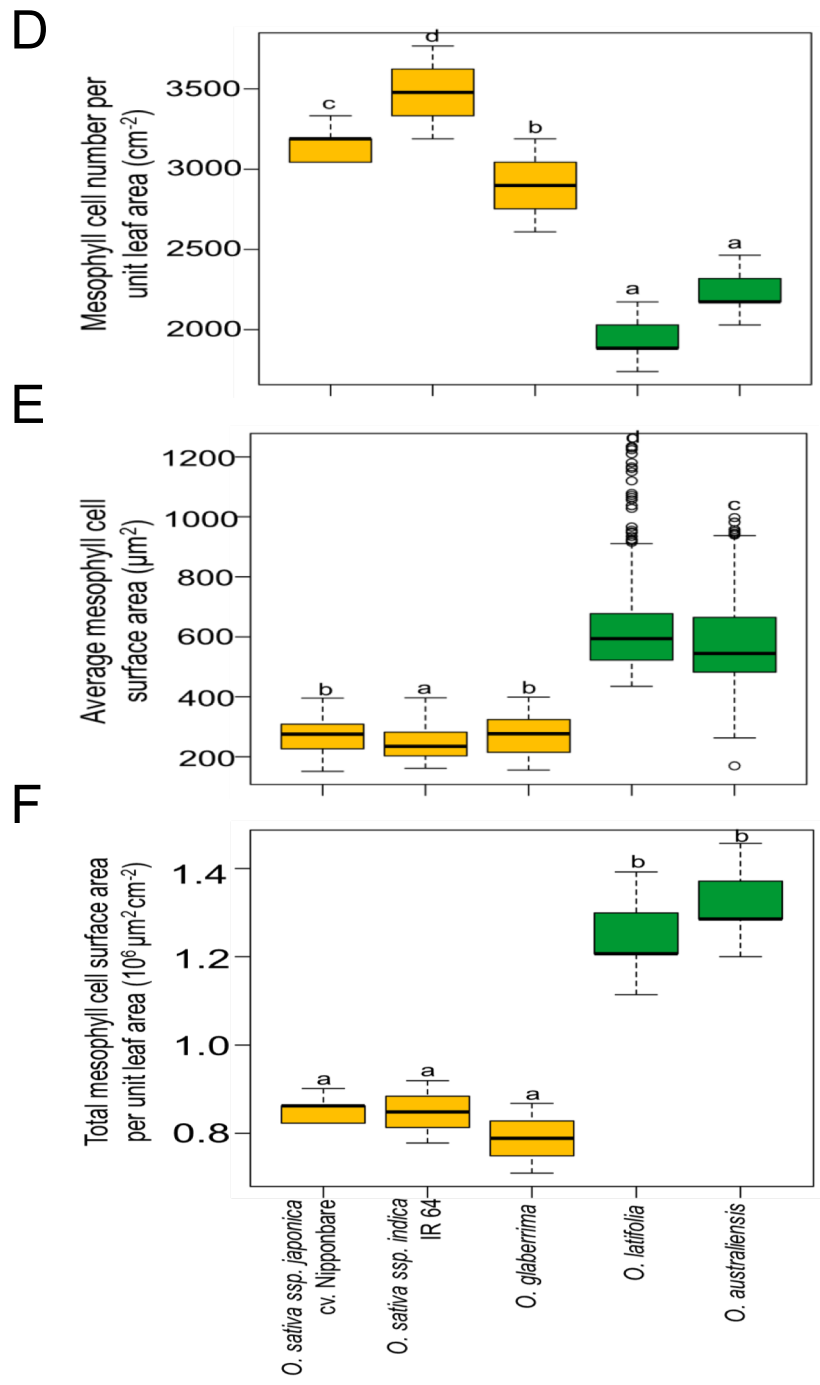

Fig. 5. Leaf developmental traits affecting photosynthesis rate and related physiological traits of rice.
(A) Correlation of leaf photosynthesis rate and related physiological traits with leaf developmental features. The red shade represents a significant positive correlation at $P \leq 0.05$.
(B) Bright-field images of a cross-section of a flag leaf of the selected genotypes showing variations in mesophyll cells and vasculature. Arrows indicate bulliform cells (bc), bundle sheath (bs), epidermis (ep), mesophyll cells (mc), and minor veins (miv). Scale bars represent 100 µm.
(C) Bright-field microscopy images showing variations in mesophyll cell features, including lobbing. Scale bar represents 10 µm.
(D-F) Quantification of total mesophyll cell number per unit leaf area (D), average mesophyll cell surface area (E), and total mesophyll cell surface area per unit leaf area (F) of selected cultivated and wild rice accessions. Cultivated rice accessions and wild species are represented with yellow- and green- shaded boxes, respectively. Each box plot shows the median and upper and lower quartiles. Different letters indicate statistical significance according to one-way ANOVA followed by post-hoc Tukey HSD calculation at $P \leq 0.05$.

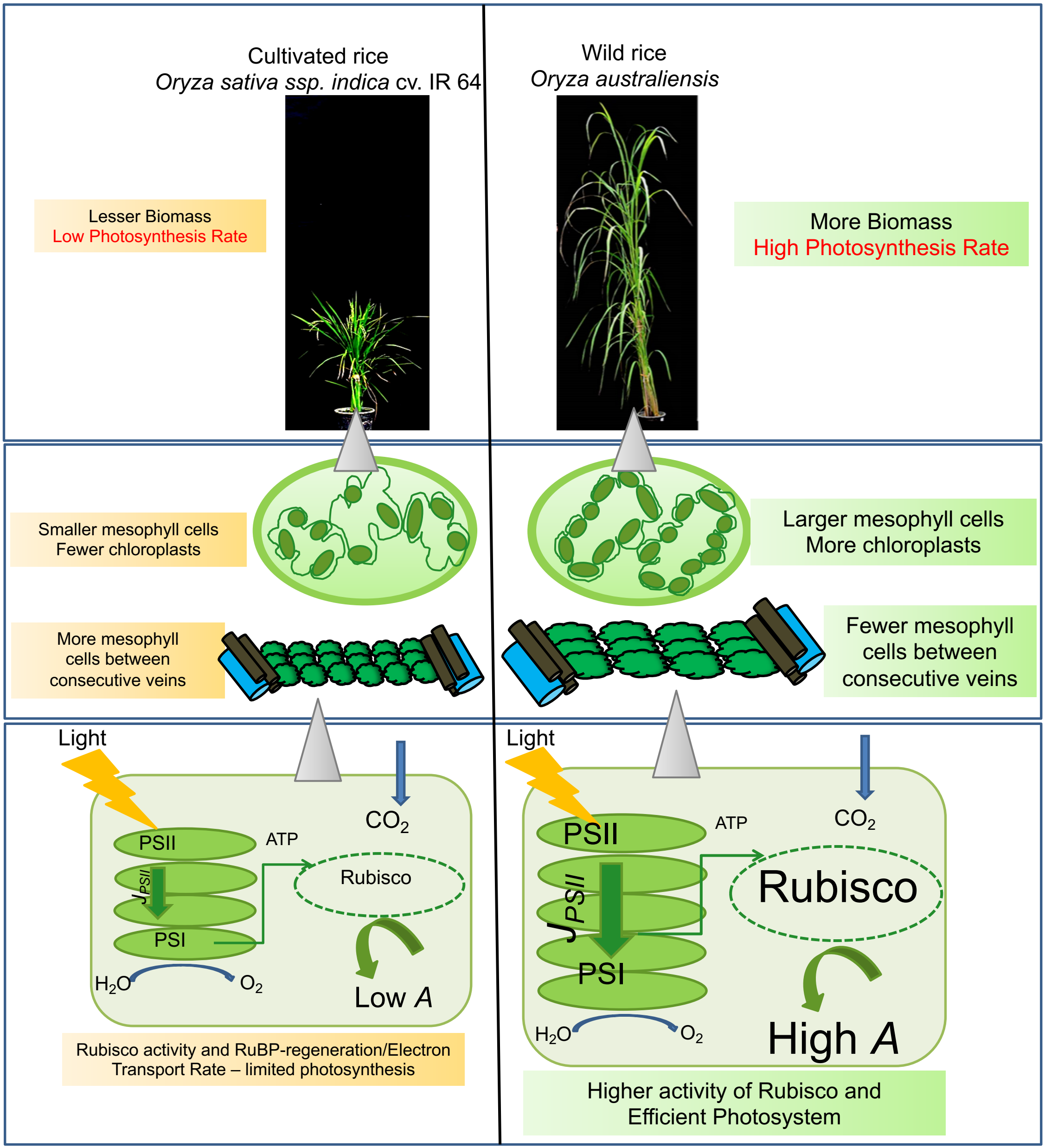

Fig. 6. Leaf developmental, photochemical, and biochemical traits contributing towards photosynthetic differences between two extreme genotypes: *Oryza sativa* ssp. *indica* cv. IR 64 and *Oryza australiensis*. Wider leaf, larger mesophyll cells, larger veins, fewer number of mesophyll cells between two consecutive veins, more chloroplasts, efficient Electron Transport Rate along with higher Rubisco activity facilitate higher leaf photosynthesis per unit area in the wild rice species *Oryza australiensis* compared to the cultivated variety *Oryza sativa* ssp. *indica* cv. IR 64.